Atmos. Meas. Tech. Discuss., 3, 1645–1705, 2010
www.atmos-meas-tech-discuss.net/3/1645/2010/

Atmospheric Measurement Techniques Discussions

This discussion paper is/has been under review for the journal Atmospheric Measurement Techniques (AMT). Please refer to the corresponding final paper in AMT if available.

Speeding up the AOT retrieval procedure using RTT analytical solutions: FAR code

I. L. Katsev[1], **A. S. Prikhach**[1], **E. P. Zege**[1], **J. O. Grudo**[1], **and A. A. Kokhanovsky**[2,1]

[1]Institute of Physics, National Academy of Sciences of Belarus, Pr. Nezavisimosti 68, 220068, Minsk, Belarus
[2]Institute of Environmental Physics, University of Bremen, O. Hahn Allee 1, 28334 Bremen, Germany

Received: 12 March 2010 – Accepted: 14 March 2010 – Published: 12 April 2010

Correspondence to: I. L. Katsev (katsev@light.basnet.by)

Published by Copernicus Publications on behalf of the European Geosciences Union.

Abstract

We present here the aerosol retrieval technique that uses radiative transfer computations in the process of retrieval rather than look-up tables (LUT). This approach provides operational satellite data processing due to the use of the accurate and extremely fast radiative transfer code RAY previously developed by authors along with approximate analytical solutions of the radiative transfer theory. The aerosol optical thickness (AOT) and Angström exponent are optimized in the iteration process using the least-squares technique with fast computations of the derivatives of radiative characteristics in respect to retrieved values. The developed technique can be adapted for processing data of various satellite instruments (including any spectral multi-angle polarization-sensitive sensors).

Beside, two important problems that determine the accuracy of the AOT retrieval are considered. The first one is the effect of the preliminary choice of the aerosol model, particularly for retrieval from satellite instrument providing only spectral data (MERIS, MODIS). The second problem is the influence of clouds in adjacent pixels. As for our knowledge, this problem has not been given required attention up to now and it should be properly accounted in the AOT retrieval algorithms.

1 Introduction

For many years all main techniques to retrieve a spectral aerosol optical thickness (AOT) from satellite data include the radiative transfer (RT) in the data processing using look-up tables (LUT). The main and evident advantage of this technique is time saving. But increasing information provided by satellite sensors (multi-angle, multi-spectral data, polarization measurements) opens the possibility to use various statistical optimizations in the satellite data processing. With this in view the use of RT calculations in the satellite data processing has a great potentiality. It is why a few years ago we started to develop the aerosol retrieval techniques that use radiative transfer

AMTD

3, 1645–1705, 2010

computations in the process of retrieval rather than LUT. The first operating algorithm of this type, the ART code for processing MERIS spectral data, was presented by Katsev et al., 2009. Another codes that use RT calculation for satellite data processing have been arrived lately as well (Kokhanovsky et al., 2009).

But such retrieval technique can be applied operationally only if the accurate and extremely fast radiative transfer procedures are used. Previously, we have developed the RAY code (Chaikovskaya et al., 1999; Tynes et al., 2001) for simulations of the radiative transfer in the atmosphere-underlying surface system with regard to polarization that meets accuracy and speed requirements. The short description of RAY was given in (Katsev et al., 2009). Recently its good accuracy along with high calculation speed was confirmed in the paper (Kokhanovsky et al., 2010). The RAY's high processing speed allows the use of the iterative radiation transfer computations in the processing of satellite data for the AOT retrieval. RAY becomes a core of our codes for the AOT retrieval.

The first successful implementation of this idea (the use of RT computations in the process of the AOT retrieval with the least-squares optimization) was the ART code for MERIS data processing outlined in (Katsev et al., 2009). Nevertheless the processing time still stays crucial for operating satellite retrieval codes dealing with huge body of information. Below we present a new FAR (Fast Aerosol Retrieval) code that has a lot of common with the previous ART code. The main difference is in the used RT procedures. Like the ART code that can be considered as a prototype, the FAR does not use the LUT technique. Unlike the ART, it includes the approximate analytical solutions for the lowest atmosphere layer characterized by the highest spatial variability, along with the RAY computations for the atmosphere above this layer. This new approach keeps main advantages of the ART technique, allowing a lot of convenient services, for instance, simple revising of atmosphere models, of aerosol composition, use of the least-squares method to find the AOT and Angström exponent from MERIS data and so on. The errors of the AOT retrieval with the FAR only slightly exceed errors providing by the ART retrieval and stay much less than inaccuracy due to other factors (a priory

choice of the aerosol model and so on). But retrieval with the FAR is about 100 times faster than with the ART technique.

Both codes can be used for the AOT retrieval for atmosphere over land and over water, but here for brevity we will consider only retrieval of the AOT over land.

This paper is arranged as following. The FAR algorithm is presented in Sect. 2. The very short description of the used atmosphere and surface models, of the procedures of the FAR code that are the same as in the ART (preparation of the input data, optimization with the least-squares technique) are given in Sect. 2.1. Because all details can be found in (Katsev et al., 2009), this section includes only information that is necessary for the understanding the FAR technique. Section 2.2 introduces the approximate analytical solution used in the FAR for calculation of the radiative characteristics of the lower aerosol layer and illustrates their accuracy. The radiative interactions between layers are considered in Sect. 2.3. Section 3 is devoted to the validation of the FAR code with the ART for benchmarking and by comparison with AERONET data. Beside, two important problems that determine the accuracy of the AOT retrieval are considered. The first one is the effect of the preliminary choice of the aerosol model, particularly for retrieval from satellite instrument providing only spectral data (MERIS, MODIS) (Sect. 4.1). The second problem is the influence of clouds in adjacent pixels (Sect. 5). As for our knowledge this problem has not been given required attention up to now and it should be properly accounted practically in all AOT retrieval algorithms.

2 Fast Aerosol Retrieval algorithm

2.1 Aerosol and surface models and brief description of the AOT retrieval

The developed FAR algorithm is designed to retrieve the AOT, Angström exponent and underlying spectral surface albedo from the top of atmosphere (TOA) spectral

AMTD
3, 1645–1705, 2010

reflectance defined as

$$R_{\mathrm{TOA}}(\lambda,\mu,\mu_0,\varphi) = \frac{\pi I_{\uparrow}(\lambda,\mu,\mu_0,\varphi)}{\mu_0 E_0(\lambda)}, \quad (1)$$

where $E_0(\lambda)$ is the extraterrestrial irradiance incident normally on a given unit area at the top-of-atmosphere, $I_{\uparrow}(\lambda,\mu,\mu_0,\varphi)$ is the measured TOA radiance, μ_0 and μ are cosines of the incidence and observation zenith angles, φ is a difference between the azimuth angles of the incidence and observation directions.

As it was mentioned above, the ART algorithm described in detail in (Katsev et al., 2009) is a prototype of the presented FAR algorithm. One can consider this FAR algorithm as a faster version of the ART. In this section we will briefly remind the features of the data processing that are common for both codes (ART and FAR) referring a reader to the abovementioned publication for the detail.

In both algorithms the model of the stratified atmosphere is taken as two coupled layers. Both layers include aerosol scattering and absorption, molecular scattering, and gas absorption. The layer "1" (lower layer) of the atmosphere is a comparatively thin layer of the lower troposphere up to the height H. As aerosol in this layer is characterized by maximal spatial and temporal variations, the AOT of this layer is supposed to vary from pixel to pixel and is retrieved for each pixel independently. Stratification in this layer is neglected. The performed computations showed that the ignorance of the stratification inside the layer "1" leads to the relative error of calculations of the reflectance at the top of atmosphere less than 0.2% for any wavelength in the visible.

The optical characteristics (optical thickness τ, single scattering albedo ω, and phase function $p(\theta)$) of this uniform layer "1" are calculated including contributions of molecular scattering, gas absorption and absorption and scattering by aerosol, namely

$$\tau = \tau_R + \tau_{\mathrm{aer}} + \tau_g, \quad (2)$$

$$\omega = \frac{\omega_R \tau_R + \omega_{\mathrm{aer}} \tau_{\mathrm{aer}}}{\tau_R + \tau_{\mathrm{aer}} + \tau_g}, \quad (3)$$

AMTD
3, 1645–1705, 2010

where τ_R , τ_{aer}, and τ_g are the optical thicknesses corresponding to molecular scattering, light extinction by aerosol particles, and gaseous absorption contributions, respectively. Equation (3) also includes the single scattering albedo of aerosol particles (ω_{aer}) and that of Rayleigh scattering processes ($\omega_R = 1$).

As for the phase function of layer "1", it is enough to calculate the coefficients x_n of the expansion of the phase function $p(\theta)$ into series of Legendre polynomials:

$$x_n = \frac{\tau_R x_{n,R} + \omega_{\text{aer}} \tau_{\text{aer}} x_{n,\text{aer}}}{\tau_R + \omega_{\text{aer}} \tau_{\text{aer}}}. \quad (4)$$

Here $x_{n,R}$ and $x_{n,\text{aer}}$ are the coefficients of the expansion of the Rayleigh and aerosol phase functions, respectively, into series of Legendre polynomials. These coefficients x_n are used in the adding method procedure to calculate the radiative interaction between layers "1" and "2". Because the Rayleigh scattering phase function comprises only the zeroth and second Legendre polynomials, we have:

$$x_n = \frac{0.5\delta_{n2}\tau_R + \omega_{\text{aer}} \tau_{\text{aer}} x_{n,\text{aer}}}{\tau_R + \omega_{\text{aer}} \tau_{\text{aer}}} \quad (5)$$

at $n \geq 1$ and also $x_0 = 1$ by definition. Here δ_{n2} is the Kronecker symbol equal to one at $n = 2$ and zero, otherwise.

The layer "2" (upper layer, i.e. the atmosphere above the altitude H) includes the stratosphere and the upper and middle troposphere. Naturally, the layer "2" is characterized by the vertical stratification of the aerosol and gases concentrations, pressure and temperature profiles. In the computation procedure, this layer is considered as composed of N homogenous sub-layers with optical characteristics averaged over each sub-layer. The optical characteristics of each sublayer are computed including contributions of molecular scattering, gas absorption and aerosol absorption and scattering similarly the procedure described above with Eqs. (2)–(5). To reduce the computation volume the radiation characteristics of the stratified layer "2" are computed one time for all pixels of the processing frame. For the layer "2", the reflectances at the illumination from the top $R_2(\mu,\mu_0,\phi)$ and from the bottom $R_2^*(\mu,\mu_0,\phi)$ as well as the

AMTD
3, 1645–1705, 2010

transmittance at the illumination from the bottom $T_2^*(\mu,\mu_0,\phi)$ are computed with the fast and accurate RAY code.

The model of the land spectral albedo $r_s(\lambda)$ is taken as a linear combination

$$r_s(\lambda) = c r_{\text{veg}}(\lambda) + (1-c) r_{\text{soil}}(\lambda) \quad (6)$$

of some basic spectra of the vegetation $r_{\text{veg}}(\lambda)$ and soil $r_{\text{soil}}(\lambda)$. These basic spectra are given by von Hoyningen-Huene et al. (2003). Thus, the spectral albedo of the surface is characterized by the only parameter c. Just this surface parameter is determined in the retrieval process. The normalized differential indices serve as a zeroth approximation for the parameter c for each pixel. This normalized differential vegetation index for the "land" pixels is defined as

$$\text{NDVI} = \frac{R(865\text{nm}) - R(665\text{nm})}{R(865\text{nm}) + R(665\text{nm})}. \quad (7)$$

The spectral radiance at the TOA measured by any satellite optical instrument in N spectral channels could be the input to the FAR (and ART) algorithms. Because both algorithms do not use the LUT technique, the choice of the spectral channels is very flexible. Their number and particular wavelengths depend on the spectral characteristics of the used satellite optical instrument. Satellite data in 9 MERIS spectral channels specified by the wavelengths

$$\lambda = 412.5, 442.5, 490, 510, 560, 620, 665, 865 \text{ and } 885\text{nm}$$

are used. These channels are hardly affected by gaseous absorption, except for the ozone absorption at wavelengths of 510–665 nm.

The flow chart and detailed description of the ART retrieval has been presented in (Katsev et al., 2009). The FAR technique differs from ART only in the radiative transfer computation procedures. It is why we refer the reader to the abovementioned paper for flow-chart and detailed description of all steps common for both codes. Here we will give only a list of the main steps of these algorithms.

The preparation of the input data includes three main steps:

1. discarding of the cloud pixels;
2. separation of the "land" and "water" pixels on the base of the NDVI values;
3. setting up the box of neighbors "good" pixels of the same type ("land" or "water").

We will additionally discuss the discarding of the cloudy pixels and design of the pixel box in Sect. 5 in connection with proposed changes in these procedures.

Radiative transfer procedures include:

1. Computations of the reflectance at the illumination from the top $R_2(\mu,\mu_0,\varphi)$ and from the bottom $R_2^*(\mu,\mu_0,\varphi)$ as well as the transmittance at the illumination from the bottom $T_2^*(\mu,\mu_0,\varphi)$ for the layer "2". These radiative transfer characteristics are computed taking into account the stratification of atmosphere and light polarization effects as a solution of the vector radiative transfer equation with the RAY code.
2. Radiative transfer for the layer "1" is computed in the FAR using analytical approximate solutions, described in Sect. 2.2 .
3. The analytical procedure to include the radiative interactions between layers "1" and "2" is presented in Sect. 2.3.
4. The iteration process with the least-squares method using the average values (over the box) $\bar{R}_{\mathrm{TOA}}(\lambda)$ in 7 spectral channels (λ = 412.5,442.5,490,510,560,620 and 665nm) is carried out. The aerosol optical thickness $\tau(\lambda)$ and Angström exponent α of layer "1", and the mixing parameter c in the model of the land spectral albedo $r(\lambda)$ are retrieved using iteration process

$$\begin{aligned}\tau_{412,\,i+1} &= \tau_{412,\,i} + \Delta\tau_{412,\,i}\\ \alpha_{i+1} &= \alpha_i + \Delta\alpha_i\\ c_{i+1} &= c_i + \Delta c_i\end{aligned} \qquad (8)$$

with the assumption

$$\tau(\lambda) = \tau_{412}\left(\lambda/412.5\right)^{-\alpha}, \tag{9}$$

where λ is measured in nm.

The corrections $\Delta\tau_{412,i}$, $\Delta\alpha_i$, Δc_i in Eq. (8) at the i-th step of iterations are determined from the following set of equations:

$$\bar{R}_{\mathrm{TOA}}\left(\lambda_j\right) = \bar{R}_{\mathrm{TOA},i}\left(\lambda_j\right) + \frac{\mathrm{d}\bar{R}_{\mathrm{TOA},i}\left(\lambda_j\right)}{\mathrm{d}\tau_{412,i}}\Delta\tau_{412,i} + \frac{\mathrm{d}\bar{R}_{\mathrm{TOA},i}\left(\lambda_j\right)}{\mathrm{d}\alpha_i}\Delta\alpha_i + \frac{\mathrm{d}\bar{R}_{\mathrm{TOA},i}\left(\lambda_j\right)}{\mathrm{d}c_i}\Delta c_i,$$
$$j = 0, 1, \ldots 7 \tag{10}$$

where $\bar{R}_{\mathrm{TOA}}\left(\lambda_j\right)$ are the satellite processed data at 7 MERIS wavelengths listed above, and values $\bar{R}_{\mathrm{TOA},i}\left(\lambda_j\right)$ are the radiances computed at $\tau_{412} = \tau_{412,i}$, $\alpha = \alpha_i$, and $c = c_i$.

The iterations (8) stop if

$$\left|\left(\tau_{412,i+1} - \tau_{412,i}\right)/\tau_{412,i}\right| \le \delta, \qquad \delta = 0.02. \tag{11}$$

The zeroth approximation for the iteration process is chosen as: $\alpha_0 = 1.3$, $\tau_{412} = 0.3$ and $c_0 = \mathrm{NDVI}$. Practice with the AOT retrieval shows that the iteration process convergence is hardly sensitive to the choice of the zeroth approximation for the parameters α and τ_{412}.

5. Calculation of the spectral optical thickness and the Angström exponent for the total atmosphere.

6. The spectral albedo of the underlying surface $r_s(\lambda)$ is calculated with the new corrected model of the troposphere aerosol and the retrieved dependence $\tau(\lambda)$. When the underlying surface is land, the surface albedo r_s is defined from the well known equation

AMTD
3, 1645–1705, 2010

$$R_{TOA}(\mu,\mu_0,\varphi) = R_a(\mu,\mu_0,\varphi) + \frac{t_a(\mu)t_a(\mu_0)r_s}{1-r_s r^*_{sa}}, \quad (12)$$

where $R_a(\mu,\mu_0,\varphi)$ is the TOA reflectance of the whole atmosphere above a black underlying surface, $t_a(\mu_0)$ is the transmission coefficient of the whole atmosphere, r_s, the surface albedo, r^*_{sa}, the spherical albedo of the atmosphere at illumination from an atmosphere bottom upwards. Eq. (12) is obtained assuming a Lambertian underlying surface. Note that Eq. (12) is accurate for the stratified atmosphere.

The listed steps and operations make the skeleton both of the FAR and ART algorithms.

2.2 Analytical radiative transfer solution used in the FAR code

To speed up satellite data processing the FAR algorithm uses approximate analytical solutions of the radiative transfer theory to calculate the reflectance $R_1(\mu,\mu_0,\phi)$ and transmission coefficient $t_1(\mu)$ for the troposphere layer "1" considered being uniform. Emphasize that radiative transfer in the layer "2" is computed accurately with the RAY code. The main difficulty in the development of the simple and sufficiently accurate approximation is the elongation of the troposphere aerosol phase function. Actually, the solution of this problem is well-known: it is the truncation of the phase function, the simplest version being known as δ – Eddington approximation. The truncation of the phase function in small angle region does not practically affect the reflectance of the layer in the backward hemisphere. Figure 1 that shows the reflectance for the aerosol layers with optical thicknesses $\tau = 0.2$ and 0.5 versus the observation angle illustrates this statement. This figure presents data for the layer with the *Continental* aerosol under the normal incidence. The calculations are performed at different truncating angles with code RAY. It is seen that even the truncation at the angle of 60° only negligibly changes the reflectance at observation angles ϑ<80°.

For the truncated phase function the reflectance from a layer can be calculated using any simple approximations developed for a not very elongated phase function with opti-

AMTD
3, 1645–1705, 2010

cal parameters $\tilde{\tau}, \tilde{\omega}, \tilde{p}(\theta)$ (the sign "~" shows that the value is defined for the truncated phase function) instead of τ, ω and $p(\theta)$. These optical parameters are defined as:

$$\tilde{\tau} = (1 - \omega\eta)\tau, \; \tilde{\omega} = \frac{\omega(1-\eta)}{1-\omega\eta}, \; \tilde{p}(\theta) = \frac{p(\theta)}{1-\eta}. \tag{13}$$

Here ω, τ, and $p(\theta)$ are the single scattering albedo, optical thickness, and phase function, θ, the scattering angle,

$$\cos\theta = -\mu\mu_0 + \sqrt{1-\mu^2}\sqrt{1-\mu_0^2}\cos\phi, \tag{14}$$

$$\eta = (1/2)\int_0^{\theta^*} p(\theta)\sin\theta \mathrm{d}\theta, \tag{15}$$

η, the truncated part of the phase function, θ^*, truncating angle. Here the phase function is normalized as $(1/2)\int_0^{\pi} p(\theta)\sin\theta \mathrm{d}\theta = 1$.

For the reflectance from a layer with the truncated phase function we use simple formulas given in (Sobolev, 1975) for not very elongated phase functions. With this solution the single scattering is computed accurately. The multiple scattering for the truncated phase function is determined the more accurate the less elongated phase function. It is why the merging of phase function truncation with this approach allows reasonably accurate computations for the layer "1". With this approximation (for the brevity let us refer to it as MSA (Modified Sobolev Approximation) in what follows) the function $R_1(\mu, \mu_0, \phi)$ is calculated as

$$R_1(\mu, \mu_0, \phi) = R_1^{(1)}(\mu, \mu_0, \phi) + R_1^{\mathrm{mult}}(\mu, \mu_0). \tag{16}$$

Here

$$R_1^{(1)}(\mu, \mu_0, \phi) = \tilde{\omega}\tilde{p}(\theta)\rho_1. \tag{17}$$

$$\rho_1 = \frac{1}{4(\mu+\mu_0)}\left(1-\exp\left[-\tilde{\tau}\left(\frac{1}{\mu}+\frac{1}{\mu_0}\right)\right]\right), \quad (18)$$

$$R_1^{\text{mult}}(\mu,\mu_0) = 1 - \frac{R(\tilde{\tau},\mu)R(\tilde{\tau},\mu_0)}{4+(3-\tilde{x}_1)\tilde{\tau}} + \left[(3+\tilde{x}_1)\mu\mu_0 - 2(\mu+\mu_0)\right]\rho_1, \quad (19)$$

$$R(\tilde{\tau},\mu) = 1 + 1.5\mu + (1-1.5\mu)e^{-\tilde{\tau}/\mu}, \quad (20)$$

$\tilde{x}_1 = 3\tilde{g}$ is the first coefficient of the expansion of the truncated scattering phase function $\tilde{p}(\theta)$ into a series of Legendre polynomials, $\tilde{g}$, the average cosine of the scattering angle for the truncated phase function.

As it is seen from Fig. 1 such truncation does not cause the noticeable errors in the computed reflection functions from the layer "1". Simultaneously it leads to the values of $\tilde{x}_1 \sim 1$ for the truncated phase functions that provide the reasonable accuracy of the used approximation. Figure 2 that compares the RAY and MSA calculations of the reflectance for the layers with optical thicknesses in the range 0–1 and for various geometries of observations illustrates this statement. The analysis shows the truncation angle $\theta^* \approx 45^\circ$ is about optimal for the estimation of the layer reflectance.

Figure 3 that presents the estimations of the MSA errors obtained by comparison with the RAY computations for different truncation angles illustrates this recommendation. The overview of the accuracy of the MSA solutions at different geometries of incidence and observation one can get from Figs. 4 and 5. The accurate reflectances for the errors estimations were computed with the RAY code. Here the azimuth angle 180° at $\mu = \mu_0$ corresponds the backscattering direction.

From these data it follows that the errors of the MSA approximation practically do not exceed 10% for $\tau < 0.5$ and observation angles $\vartheta < 60^\circ$. One can expect that errors of the optical thickness retrieval due to the use of this approximation are less than 10% as well. The largest values of error occur near the directions of the mirror reflection at low Sun position (Sun and observation angles more than 60°, azimuth angle 0°). But this geometry practically is not used in satellite observations. Note that black areas in

Figs. 4 and 5 where we even do not estimate the errors of the MSA include only these regions.

2.3 Radiative interaction between the atmosphere layers in the FAR code

To compute the atmosphere TOA reflectance $R_a(\mu,\mu_0,\varphi)$ in Eq. (12) one should include the radiative interaction between the lower ground layer "1" and upper layer "2" of the atmosphere. The following equation describes this interaction correctly enough:

$$R_a(\mu,\mu_0,\phi) = R_2(\mu,\mu_0,\phi) + T_2^* * R_1 * T_2 + \frac{t_2(\mu) r_1^2 r_2^* t_2(\mu_0)}{1 - r_2^* r_1}. \quad (21)$$

Here $R_1(\mu,\mu_0,\phi)$ and $R_2(\mu,\mu_0,\phi)$ are reflectance from the layers "1" and "2" correspondingly when illuminated from above, $T_2(\mu,\mu_0,\phi)$ and $T_2^*(\mu,\mu_0,\phi)$ are the transmission functions for the layer "2" while illuminated from above and below correspondingly, $t_2(\mu_0) = \frac{1}{\pi}\int_0^{2\pi} d\phi \int_0^1 T(\mu,\mu_0,\phi)\mu d\mu$, the transmission coefficient for the directional illumination, $r_1 = 2\int_0^1 \mu d\mu \frac{1}{\pi}\int_0^{2\pi} d\phi \int_0^1 R_1(\mu,\mu_0,\phi)\mu_0 d\mu_0$ and $r_2^* = 2\int_0^1 \mu d\mu \frac{1}{\pi}\int_0^{2\pi} d\phi \int_0^1 R_2^*(\mu,\mu_0,\phi)\mu_0 d\mu_0$, the spherical albedo of the layers "1" and "2" while illuminated from above and below correspondingly. The sign $*$ in the equation $Z = X * Y$ denotes the integral convolution of two functions (Lenoble et al., 1985):

$$Z(\mu,\mu_0,\varphi-\varphi_0) = \frac{1}{\pi}\int_0^{2\pi} d\varphi' \int_0^1 X(\mu,\mu',\varphi-\varphi') Y(\mu',\mu_0,\varphi'-\varphi_0) d\mu', \quad (22)$$

i.e.

$$T_2^* * R_1 * T_2 = \frac{1}{\pi^2}\int_0^{2\pi} d\phi' \int_0^1 T_2^*(\mu,\mu',\phi-\phi') d\mu' \int_0^{2\pi} d\phi'' \int_0^1 R_1(\mu',\mu'',\phi'-\phi'') T_2(\mu'',\mu_0,\phi''-\phi_0) d\mu'' \quad (23)$$

AMTD
3, 1645–1705, 2010

In Eq. (21) there is taken into account that non-Lambertian reflection from the layer "1" is essential only at the first interaction with Sun radiation transmitted by the layer "2". While considering the multiple re-reflections between layers one can consider that the layers are illuminated by the diffuse light.

Let us note that the following relations

$$R_a(\mu,\mu_0,\phi) = R_2(\mu,\mu_0,\phi) + \frac{t_2(\mu)\, r_1\, t_2(\mu_0)}{1 - r_2^* r_1}, \tag{24}$$

$$R_a(\mu,\mu_0,\phi) = R_2(\mu,\mu_0,\phi) + \frac{t_2(\mu) R_1(\mu,\mu_0,\phi)\, t_2(\mu_0)}{1 - r_2^* r_1} \tag{25}$$

are used comparatively frequently instead of Eq. (21). These relations are simpler than Eq. (21). But Eq. (24) is correct only in the assumption of the Lambertian distribution of the reflectance $R_1(\mu,\mu_0,\phi)$. It is clear that Eq. (25) is also correct in this particular case. Besides, this relation is the more accurate the narrower angular distributions of the light transmittance $T_2(\mu,\mu_0,\phi)$. Our computations have shown (Katsev et al., 2009) that the assumption (25) can lead to the noticeable errors in the computations of the whole atmosphere reflectance $R_a(\mu,\mu_0,\phi)$. Overestimations and underestimations of this value are both possible. The error depends on the Sun position, observation angle, and wavelength and so on.

To use Eq. (21) and to keep the advantages of our analytical approach providing the FAR processing speed, let us take the function $T_2(\mu,\mu_0,\phi)$ as a sum of the direct $t_2^0(\mu_0)\delta(\varphi)$, and scattered $t_2^{\mathrm{dif}}(\mu,\mu_0,\phi)$ parts, i.e.:

$$T_2(\mu,\mu_0,\phi) = t_2^0(\mu_0)\delta(\varphi) + t_2^{\mathrm{dif}}(\mu,\mu_0,\phi). \tag{26}$$

Then

$$\begin{aligned} T_2^* * R_1 * T_2 &= t_2^0(\mu) R_1(\mu,\mu_0,\phi) t_2^0(\mu_0) \\ &+ \left(t_2^{*\mathrm{dif}} * R_1\right) t_2^0(\mu_0) + t_2^0(\mu)\left(R_1 * t_2^{\mathrm{dif}}\right) + t_2^{*\mathrm{dif}} * \left(R_1 * t_2^{\mathrm{dif}}\right) \end{aligned} \tag{27}$$

AMTD
3, 1645–1705, 2010

and from (21) it follows:

$$R_a(\mu,\mu_0,\phi) = R_2(\mu,\mu_0,\phi) + \frac{t_2(\mu) r_1^2 r_2^* t_2(\mu_0)}{1 - r_2^* r_1} + \left[t_2^0(\mu) R_1(\mu,\mu_0,\phi) t_2^0(\mu_0) + \left(t_2^{*\mathrm{dif}} * R_1 \right) t_2^0(\mu_0) + t_2^0(\mu) \left(R_1 * t_2^{\mathrm{dif}} \right) + t_2^{*\mathrm{dif}} * \left(R_1 * t_2^{\mathrm{dif}} \right) \right]. \quad (28)$$

In Eq. (28) it is regarded that the angular distribution of the transmitted scattered light is not narrow.

For the convolution integral in Eq. (28) we have:

$$t_2^{*\mathrm{dif}} * R_1 \approx 2 \sum_{k=0}^{N} A_k \mu'_k t_2^{*\mathrm{dif}}(\mu,\mu'_k) \bar{R}_1^{\phi}(\mu'_k,\mu_0)$$
$$R_1 * t_2^{\mathrm{dif}} \approx 2 \sum_{k=0}^{N} A_k \mu'_k \bar{R}_1^{\phi}(\mu,\mu'_k) t_2^{\mathrm{dif}}(\mu'_k,\mu_0) \quad , \quad (29)$$

where μ'_k and A_k are the nodes and weights of the Gaussian quadratures, $\bar{R}_1^{\phi}(\mu,\mu_0)$ is the azimuth averaged reflectance $R_1(\mu,\mu_0,\phi)$.

The function $\bar{R}_1^{\phi}(\mu,\mu_0)$ with regard to Eqs. (16) and (13) can be written as a sum of the single and multiple scattering components as

$$\bar{R}_1^{\phi}(\mu,\mu_0) = \overline{R_1^{(1)}(\mu,\mu_0,\phi)}^{\phi} + R_1^{\mathrm{mult}}(\mu,\mu_0) = \tilde{\omega}\tilde{p}(-\mu,\mu_0)\rho_1 + R_1^{\mathrm{mult}}(\mu,\mu_0), \quad (30)$$

where

$$\tilde{p}(-\mu,\mu_0) = \sum_n \tilde{x}_n P_n(-\mu) P_n(\mu_0), \quad (31)$$

$\tilde{x}_n$ are coefficients of the expansion of the truncated scattering phase function $\tilde{p}(\theta)$ into a series of Legendre polynomials.

The transmission coefficient $t_a(\mu_0)$ of the atmosphere (see Eq. (12)) defined with regard to multiple re-reflections between layers "1" and "2" can be given by the following

approximate relation:

$$t_a(\mu_0) \approx t_2^0(\mu_0) t_1(\mu_0) + t_2^{dif}(\mu_0) t_1(\mu_0 = 0.5) + \frac{t_2(\mu_0) r_1 r_2^*}{1 - r_1 r_2^*} t_1(\mu_0 = 0.5), \quad (32)$$

where

$$t_2^{\text{dif}}(\mu_0) = t_2(\mu_0) - t_2^0(\mu_0), \quad (33)$$

and the transmission coefficient of the layer "1" can be taken as

$$t_1(\mu_0) = \exp\left[-\tilde{\tau}_1 \left(1 - \tilde{\omega}_1 \tilde{F}_1\right) / \mu_0\right], \quad (34)$$

where

$$\tilde{F}_1 = 1 - \frac{1 - \tilde{g}_1}{2}. \quad (35)$$

Figure 6 illustrates the accuracy of this approximation presenting the comparison between the angular dependencies of the transmission coefficients $t_1(\mu_0)$ computed with Eqs. (34)–(35) and with the RAY code. Data for the different values of the optical thickness τ_1 of the layer "1" and for the aerosol models *Continental* and *Water-soluble* are presented. It is seen that at $\tau_1 < 0.5$ and $\vartheta < 70^0$ the error of the approximation (34) is less than 5%.

Now let us consider the accuracy of Eqs. (32)–(34) that define the transmission coefficient $t_a(\mu_0)$ of the atmosphere. As it is seen from Fig. 7, these simple solutions provide the reasonable accuracy for the computations of the atmosphere transmission coefficients. Thus, with the obtained approximations we got the reasonable accuracy for the atmosphere TOA reflectance $R_a(\mu, \mu_0, \varphi)$ in Eq. (12) that gives the TOA reflectance $R_{\text{TOA}}(\mu, \mu_0, \varphi)$ from the atmosphere-underlying surface system.

Equation (12) includes one more value that requires the attention. It is the spherical albedo of the atmosphere at illumination of atmosphere from bottom upwards r_{sa}^*. As it is seen from Eq. (12) this value gives only a small correction to the value of the radiance

AMTD
3, 1645–1705, 2010

$R_{\mathrm{TOA}}(\mu,\mu_0,\phi)$ and it is enough to get an approximate estimation of this value. Because the layer "1" is considered as uniform, we can approximately assume that

$$r^*_{s,a} \approx r_{s,1} + \frac{t_1^2(\mu_0 = 0.5) r^*_{s,2}}{1 - r^*_{s,2} r_{s,1}}. \tag{36}$$

Here $r_{s,1}$ is the reflection coefficient for the layer "1" under the diffuse illumination, $r^*_{s,2}$ is the reflection coefficient for the layer "2" under the diffuse illumination from below. For diffuse illumination let us use the following approximations (Zege et al., 1991):

$$r_{s,1} \approx \frac{\tilde{\tau}_1}{\tilde{\tau}_1 + 4/(3 - \tilde{x}_1)} \tag{37}$$

for the layer "1" and

$$r^*_{s,2} \approx \frac{\tau_2}{\tau_2 + 4/3} \tag{38}$$

for the upper layer "2" with the governing Rayleigh scattering. Formulas (37) and (38) are accurate for the case of quasi-diffusion illumination of the homogeneous layer (Zege et al., 1991). Nevertheless, we use them for diffusion illumination because, we deal with comparatively weekly absorbing layers (when the quasi-diffusion radiance distribution is close to the diffusion one). Beside as it was mentioned above, we need to get only an approximate estimation of the value r^*_{sa} by Eqs. (36)–(38).

Thus, dividing the transmission function $T_2(\mu,\mu_0,\phi)$ of the light transmitted by the layer "2" onto the direct $t_2^0(\mu_0\delta(\varphi))$ and scattering $t_2^{\mathrm{dif}}(\mu,\mu_0,\phi)$ components allowed us to get the approximate solution without the requirement of the narrow angular distribution of $T_2(\mu,\mu_0,\phi)$ in Eq. (25).

3 Comparisons of the FAR retrievals with the ART and AERONET data

The ART retrieval was previously carefully checked by comparing with the retrieval results of other known algorithms and with AERONET data (Katsev et al., 2009). In

so doing, we used the data of the inter-comparison described in (Kokhanovsky et al., 2007). In this work the performance of different algorithms was tested for a site in Europe, where multiple and near-simultaneous satellite data were available. As many as ten different algorithms for the AOT retrieval that used data taken by six satellite optical instruments currently operated in space were compared. The explored site included the cloudless ground scene in central Europe (mainly, Germany) on 13 October 2006 (10:00 UTC). The latitude range was 49° N–53° N and the longitude range was 7° E–12° E. The results of comparing the AOT retrieved with the ART and with other algorithms can be found in (Katsev et al., 2009). They showed that the ART data are in a good agreement with results of MISR JPL, MODIS NASA, MERIS BAER, and MERIS ESA retrieval algorithms.

Several AERONET instruments operated in the area at the time of satellite measurements. We also compared the ART retrieval with AERONET data. Fig. 8, where the ART retrieval data are plotted versus AERONET data for $\lambda = 440$nm, 550nm, and 670nm, demonstrates satisfactory agreement. AERONET AOT data at 550 nm are obtained by interpolation between $\lambda = 440$nm and $\lambda = 670$nm. The ART values of the AOT at $\lambda = 412.5$nm and the Angström exponent are directly retrieved, the values of AOTs at other wavelengths, including $\lambda = 550$nm and $\lambda = 670$nm, are calculated through these values.

Thus, the accuracy of the ART, where the code RAY is used to compute the radiative transfer through atmosphere, is more than satisfactory at least for available body of satellite information (the MERIS retrieval was considered). Now we can use the ART retrieval for the FAR benchmarking. Actually, in so doing we primarily check how the use of the approximate analytical description of the radiative transfer in the layer "1" affects the accuracy of the AOT retrieval. Figure 9 presents satellite RGB images obtained from European ENVISAT platform on 11 October 2005 (left) and 1 May 2006 (right). The territories of Belarus, Baltic countries and Poland are seen in the left picture. It is the anticyclone conditions, the weather is fine, atmosphere is clear. The right image shows the territories of Belarus and west Russia. In this particular day (1 May

2006) the fire smocks caused high atmosphere turbidity. Figure 10 presents the AOT distribution over presented in Fig. 9 regions retrieved with the FAR code.

Figures 11 and 12 show very good correlation between values of the AOT retrieved with the algorithms ART and FAR using MERIS on ENVISAT data for the area specified in Fig. 9. But for small values of the AOT ($\tau < 0.5$) the FAR retrieval provides somewhat overestimated AOT values. On the contrary, at $\tau > 0.5$ the FAR retrieval leads to small underestimations of the retrieved AOT values. It is seen evidently from Figs.13 and 14 where the histograms of the distributions of the optical thickness at the wavelengths 412.5nm and 550nm are shown. The reason of these deviations is evident: it is approximate nature of analytical formulas used in the FAR for the description of the radiative transfer in the layer "1". The accuracy of this approximation depends on the optical thickness of the layer "1" and the observation geometry. Nevertheless, values of the AOT retrieved with the FAR technique differ from the correspondent the ART retrieved AOT values no more than 15–20%. This deviation is the payment for the retrieval fastness.

Let us now consider the correlation of both the FAR and ART retrieval with AERONET measurements. Figure 15 shows this comparison using data of the AERONET stations in Minsk, Belsk, Toravere, and Moscow. The ART and FAR results are pretty close and agree with AERONET data. At small AOT values of the FAR retrieval show the same bias as was observed earlier. Figure 15 depicts some bias even for the ART retrieval.

To conclude this section, let us underline the FAR potentialities as a tool for the atmosphere correction and retrieval of the land spectral albedo. The correlations between spectral albedo retrieved with the ART and FAR codes for the wavelengths 412.5nm and 560nm are depicted in Figs. 16 and 17. Practically both codes retrieve the same values of spectral albedo. This conclusion seems to be important because it emphasizes the potentialities of the FAR code for atmosphere correction of satellite images. It is important that the FAR noticeably speeds up data processing in comparison with the ART. Processing time for 10^6 pixels at ordinary PC with the dual-core processor (Intel Core 2 Duo E6600, 2.4 GHz) is about 3 h with the ART and 2 min with the FAR. Thus,

AMTD
3, 1645–1705, 2010

the FAR is about 100 times faster than the ART.

4 Importance of the choice of the aerosol model

As mentioned above, a very important issue is a priori choice of the aerosol model of the layer "1" particularly for the satellite optical sensors providing only spectral information. This model assumes not only the value of the single scattering albedo, but, what is the most important, the phase function as well. We have already touched this problem in (Katsev et al., 2009) but it needs more detail consideration and clear understanding. In this section we will consider how a priori choice of aerosol model effects the retrieved AOT and spectral surface signatures.

4.1 Influence of the aerosol model on the retrieved AOT

Preliminary choice of aerosol model is a necessary step in any AOT retrieval algorithm. The correction of this model in the process of the retrieval depends on the information, provided by satellite instrument, a priori information about local aerosol and the used retrieval technique. In all cases the preliminary choice of aerosol model effects the retrieval. This influence is the more important the less information is provided by the satellite sensor. Hence, it is particularly important for the satellite sensors providing only spectral information (MERIS, MODIS). In this section we will consider just this case.

Let us estimate the influence of the predefined phase function on the retrieved AOT values. Figure 18 demonstrates the phase functions of the aerosol models *Continental*, *Water-Soluble* and *Oceanic* at $\lambda = 550$ nm and the phase function that was measured earlier in Germany (von Hoyningen-Huene et al., 2003) (we will refer to it as the *experimental* phase function). This phase function is used, for instance, in the retrieval code BAER (von Hoyningen-Huene et al., 2003). As seen, in the angle range $\sim 100 \div 150$ deg mainly used for the AOT retrieval the values of this *experimental* phase

AMTD
3, 1645–1705, 2010

function are about two times larger than the values of the *Continental* phase function.

Values of the AOT retrieved with the ART algorithm with these two different aerosol models (*Continental* and *experimental*) are compared in Fig. 19. In what follows we will mainly use the retrieval with the ART technique as more accurate. The *experimental* model is rather simple: the single scattering albedo is equal to 0.9 (as for the *Continental* model) and the phase function is considered as independent of the wavelength. The correlation between these data is rather high, but the AOT values retrieved with the *experimental* phase function are in 1.5 times smaller.

This difference is easy to understand. Let us consider the simplest case of a small AOT, when the single scattering approximation can be used. In this case the reflectance of the aerosol layer "1" is proportional to the product of the single scattering albedo ω, phase function $p(\theta)$, and the AOT τ, i.e.

$$R_2(\mu,\mu_0,\varphi) \sim \omega p(\theta)\tau. \quad (39)$$

It means that, for example, a twofold increase of the value of the phase function $p(\theta)$ in considered direction leads to a twofold decrease of the retrieved values of the AOT. Thus, the choice of the model of the troposphere aerosol in the layer "1" can considerably affect the retrieved AOT values.

In (Kokhanovsky et al., 2009) the following computer experiment is described. The spectral response of the atmosphere with the black underlying surface was computed with the SCIATRAN code for chosen atmosphere model and a few values of the AOT. The computed spectral reflectance simulated signals registered by satellite sensors. The simplest case of the black underling surface was considered. Then, the spectral AOT was retrieved with different retrieval techniques using these simulated spectral reflectance. The atmosphere model and particularly aerosol microphysical (and optical) properties used in simulations of the radiances at the atmosphere top were kept unknown for the retrievers. The results that are the AOT retrieved by different groups with different techniques are given in (Kokhanovsky et al., 2009).

The results of such retrieval for three aerosols models (*Continental*, *Water-soluble*, *Oceanic*) are depicted in Fig. 20 dependent on the reference AOT. The phase func-

tions for these aerosol models at λ =550 nm are given in Fig. 18. As seen, these phase functions are very different, particularly *Oceanic* and *Water-soluble* in the angular range 100°–150° typical for the satellite remote sensing. It is clear that just this difference provides such discrepancy of the retrieved AOT values. The retrieval with aerosol *Oceanic* is very close to the reference values in the computer experiment.

Now let us consider the results of the following computer experiment. The spectral reflectance at the top of atmosphere were calculated with the accurate code RAY for the atmosphere models used for the retrieval for two cases (*Oceanic* and *Water-soluble* aerosols) with correspondent retrieved values of the AOT. The results are presented in Fig. 21. Let us note that the atmosphere model (that includes models of the molecular atmosphere, gases, stratification of all components) used for the AOT retrieval could essentially differ from the model used for the simulation of the satellite data. But as seen from Fig. 21 the calculated spectral reflectance for both used aerosol models do not differ and coincide with the spectral reflectance at the top of atmosphere, simulated with unknown atmosphere model.

From results of the described computer experiments it follows:

1. The spectral dependence of the reflectance measured at the TOA in the visible and near IR does not contain enough information for the uniquely choice of the aerosol model even when spectral reflectance of the underlying surface is given. At least, the spectral measurements in the range 400–900nm can not be used to recognize the aerosol type (Kokhanovsky et al., 2009). In this paper was mentioned that there is a chance that the aerosol type can be better constrained if shortwave IR measurements are used.

2. In the best case the spectral dependence of the TOA reflectance can allow one to determine some parameters of the aerosol model if this model is chosen a priori.

3. A priory choice of the aerosol model affects noticeably the retrieved value of the AOT.

AMTD
3, 1645–1705, 2010

4.2 Influence of the aerosol model on the retrieved surface albedo

One of the most important problems of satellite remote sensing is the retrieval of the true spectral albedo $r_s(\lambda)$ of the underlying surfaces (atmospheric correction). After retrieving $\tau(\lambda)$ the spectral albedo $r_s(\lambda)$ of the underlying Lambertian surface can be simply calculated from Eq. (12) if the surface is land:

$$r_s = \frac{R_{\mathrm{TOA}}(\mu,\mu_0,\varphi) - R_a(\mu,\mu_0,\varphi)}{t_a(\mu)t_a(\mu_0) + r^*_{\mathrm{sa}}\left[R_{\mathrm{TOA}}(\mu,\mu_0,\varphi) - R_a(\mu,\mu_0,\varphi)\right]}. \quad (40)$$

Let us study how the choice of the aerosol model, particularly, the aerosol phase function, influences the spectral surface albedo retrieval. The comparison of the spectral surface albedo for two wavelengths retrieved with *Continental* and *experimental* phase functions is shown in Fig. 22. The correlation of these data is very high.

Hence, the following important conclusion results from this study: the retrieved spectra of the surface albedo are comparatively stable whereas the retrieved values of the AOT are sensitive to the choice of the aerosol model. This insensitivity of the retrieved spectra of the surface albedo to variations of the aerosol phase function $p(\theta)$ follows immediately from the fact that the reflectance of layer "1" is proportional to the product of the phase function $p(\theta)$ and AOT (see Eq. 39). This statement is more accurate as the optical thickness of the layer "1" is smaller. Indeed, for a thin layer a twofold increase of the value of the phase function $p(\theta)$ in the considered direction leads to a twofold decrease of the retrieved values of the AOT. The product $p(\theta)\tau$ and the value of $R_a(\mu,\mu_0,\varphi)$ in Eq. (40) change only slightly. At small AOT such changes of τ lead to modest variations of the transmission coefficient $t_a(\mu)$.

5 Estimation of influence of adjacent cloudy pixels on the retrieved AOT value

In our ART and FAR algorithms the pixels with $R_{\mathrm{TOA}}(560) \geq 0.4$ or $\xi = R_{\mathrm{TOA}}(412)/R_{\mathrm{TOA}}(443) \leq 1.16$ are considered as containing clouds and discarded. The

first inequality immediately discards pixels containing comparatively thick clouds. The choice of the often used threshold criterion as $R_{\mathrm{TOA}}(560) \geq 0.2$ might lead to discarding not only cloud pixels, but pixels with highly reflective surfaces (for instance, sands, deserts). However, the choice of the threshold criterion as $R_{\mathrm{TOA}}(560) \geq 0.4$ does not guarantee discarding pixels containing sub-pixel clouds. In the ART and FAR codes the second criterion $\xi \leq 1.16$ is included to solve this problem at least partially. The estimations show that the use of this criterion leads to discarding pixels where clouds with the reflectance more than 0.2 cover 20% and more of the pixel area.

In our algorithms additional precaution against a bias of the retrieved AOT value due to the influence of clouds or of bright adjacent pixels is provided by the following procedure. The box of neighbors "good" pixels of the same type ("land" or "water") is set up. The box size depends on the spatial resolution of the deployed satellite instrument, number of pixels in the processing image, the scenario, and the problem under consideration. For this box the average value of $\bar{R}_{\mathrm{TOA}}(\lambda)$ is calculated. In doing so 20% of the pixels with minimal values of $R_{\mathrm{TOA}}(665\mathrm{nm})$ and 30% of the pixels with maximal values of $R_{\mathrm{TOA}}(665\mathrm{nm})$ are discarded from the data to be averaged. The determined average value of $\bar{R}_{\mathrm{TOA}}(\lambda)$ is ascribed to the central pixel in the box.

This averaging procedure implies that the optical characteristics of the aerosol layers are practically the same for all pixels in the compiled pixel box, i.e. the scale of the spatial changes of the aerosol parameters is much larger than the pixel size. It decreases the effects of the random errors of the measurements and of the small-scale variations of the surface albedo. Displacement of the pixel box by one column or one row in the array of the image frame provides retrieval of the moving-average value of the AOT in the retrieval procedure. Discarding pixels with maximal and minimal values of $R_{\mathrm{TOA}}(665\mathrm{nm})$ in the compiled pixel box from the averaging procedure allows one to eliminate or at least to decrease the effect of pixels which either partially contain clouds (maximal values of $R_{\mathrm{TOA}}(665\mathrm{nm})$) or include cloud shadows (minimal values of $R_{\mathrm{TOA}}(665\mathrm{nm})$).

Thus, the pixels with light soil (sand), snow and cloud are discarded, i.e. they are not

included in the estimation of the average value of $\bar{R}_{TOA}(\lambda)$ for the box. Nevertheless these pixels can affect signals registered from adjusted pixels because of spreading of the scattered light in atmosphere. The problem of the influence of adjacent pixels is well-known. Estimations given in (Dave, 1980; Kaufman, 1985) has shown that influence of adjacent pixels on the signal registered from the chosen pixel extends at the distance about 5 km because of molecular and aerosol scattering in atmosphere. Nowadays this feature is taken into account in the procedures of the in-flight calibration of satellite sensors, and particularly for the in-flight calibration of sensors with a high spatial resolution (Richter, 1997). Let us underline that for the AOT retrieval from satellite data with the spatial resolution about 1 km the small-scale variations of the surface albedo with small spatial fluctuations are efficiently averaged and do not make a noticeable influence. The large-scale spottiness with high albedo (clouds, snow) may affect a measured value of the AOT. In our ART and FAR algorithms (like in the MODIS algorithm (Kaufman et al., 1997) this undesirable effect is somewhat softened by discarding 30% of the pixels with maximal values of $R_{TOA}(665\,\text{nm})$ from the data to be averaged over a pixel box. But this procedure may occur insufficient.

The AOT value retrieved with the ART using MERIS data for regions of Belsk (Poland) (Fig. 23, left part) and Zvenigorod (Russia) (Fig. 24, left part) averaged over a circle with the radius of 20 km with the center in the pixel where AERONET measurements were performed are depicted at the left figures. Different signs are given for different cloud situations. We distinguish the situations with numbers of pixels identified as cloudy less than 10%, in range 10–50%, and more than 50% in the considered circle with the radius 20 km. The lines show the linear regression between AERONET data and the retrieved AOT values for the corresponding cloudy situations. Table 1 shows the coefficients of the linear regression. As seen, the more nearby cloudy pixels the higher the retrieved AOT values and the AOT dispersion.

The most likely that the influence of the cloudy pixels (to be more explicit, the pixels identified as cloudy) onto signals from adjusted pixels through the scattering in atmosphere causes this tendency. To check this assumption let us estimate the scale of "the

effect of adjacent cloudy pixels".

This scale is determined by the dispersion of the Point Spread Function (PSF) for the light propagating through the atmosphere. Just this value determines the effective square of land area that contributes in the signal registered from a pixel by a satellite instrument. The area where the contribution from adjacent pixels is noticeable is practically the same for the case of the contribution of adjacent cloudy pixels or from land pixels (see Appendix).

The dispersion of the PSF for the beam propagating through atmosphere due to aerosol and molecular scattering is estimated in the Appendix A. As it follows from estimations the presence of a cloud (snow, sand with high albedo) in some pixel affects signals registered from the nearby pixels up the distance about 1 km because of the scattering in aerosol atmosphere and at a few kilometers because of molecular scattering. This influence is expected to be more pronounced in the shortwave part of spectrum with the increasing the contribution of the molecular scattering.

With the goal to decrease the bias of the retrieved AOT due to the impact of the nearby cloudy pixels in the signal from the pixel under retrieval we included discarding not only cloudy pixels but nearby pixels as well in the retrieval algorithm. The obtained data are given in right parts of Figs. 23 and 24. The coefficients of the linear regression between AERONET data and the retrieved AOT values for this case are shown in Table 2. Thus, the only difference between the left and right parts of Figs. 23 and 24 is that values of AOT presented in right parts are obtained with the additional discarding of the pixels in the square 5×5 with the center in the cloudy pixel. Of course, this procedure decreases the number of used pixels in a box. As it was expected, the AOT values retrieved with this additional discarding decrease in comparison with data obtained without this additional discrimination and show better agreement with AERONET data. This correction is more pronounced for the situations with larger cloud fractions. Thus, one can see that the presence of clouds in the nearby pixels could provide noticeable bias of the retrieved AOT values, namely provide overshot AOT value. Let us note that this error is not less than, for instance, the errors due to the use of approximate

AMTD
3, 1645–1705, 2010

equations in the proposed express-algorithm FAR.

As it is seen from Figs. 23 and 24, the proposed method to decrease the bias of the retrieved AOT values due to effect of nearby cloudy pixels by discarding pixels adjacent to this cloudy pixel, is efficient enough. But it does not eliminate this effect completely. Beside this technique leads to some decrease of the number of pixels for retrieval. The further development of the way to eliminate this bias is desirable.

6 Conclusions

We have presented in this paper a new FAR technique for the acquisition of the atmosphere spectral AOT and spectral reflectance of the underlying surface from MERIS data. This FAR code may be considered as a faster version of the previously published ART technique (Katsev et al., 2009). These both codes include radiative transfer computations in the process of the retrieval instead of the LUT and use the least-squares method to determine the AOT and Angström exponent. The base of the both approaches is the accurate and extremely fast radiative transfer code RAY for simulation of the radiative transfer in the atmosphere-underlying surface system with account for the light polarization. The FAR code keeps all advantages of the ART technique. The main difference between ART and FAR techniques is in the radiative transfer procedures. To speed up satellite data processing and to provide operational mode the FAR code uses the combination of RAY calculations and analytical solutions of the radiative transfer theory. The FAR spectral AOT retrieval is carefully checked with ART retrievals and with available ARONET data and found to be satisfactory. Beside FAR is shown to be an efficient and accurate tool for the atmosphere correction and retrieval of the land spectral albedo. It is important that the FAR noticeably speeds up data processing in comparison with the ART

In this paper we introduced the MSA that merges the truncation of the phase function with simple solutions given in (Sobolev, 1975). The MSA accuracy is checked carefully. This approximation is used only for the computations of the radiative characteristics of

the boundary layer of troposphere.

Two more problems of the AOT retrieval are considered. First, we proceeded with estimations of the influence of a priory information about aerosol in the boundary layer on the results of the AOT retrieval from spectral satellite data. The second problem is the influence of clouds in adjacent pixels on the retrieved AOT from cloudless pixels. As for our knowledge, this problem has not been given required attention up to now. The bias in the retrieved AOT due to the clouds in adjacent pixels is confirmed using satellite data. With the goal to decrease this bias, we included discarding not only cloudy pixels but pixels adjacent to the cloudy pixels as well. This procedure decreases the AOT bias noticeably. Nevertheless, the further development in this direction is recommended.

Appendix A

Estimation of the dispersion of the point spread function for the light propagating through atmosphere

Let us estimate the dispersion of the Point Spread Function (PSF) for the light propagating through atmosphere. Just this value determines the effective neighboring area that contributes in the signal registered from a pixel by a satellite instrument. From what follows it is becomes clear that the area, where the contribution from adjacent pixels is noticeable, is practically the same for the case of the contribution of adjacent cloudy pixels or land pixels. But it is evident that the higher albedo of adjacent pixels the more they contribute to the signal from the pixel under retrieval. To estimate the dispersion of the PSF let us use the small-angle approximation (SAA) of the radiative transfer theory (Zege et al., 1991) that allows for atmosphere stratification. Note, that the SAA is developed for the scattering media with strongly elongated phase functions and strictly speaking cannot provide good accuracy in the case of the molecular scattering. Nevertheless, because we are interested only to get some rough estimation of the PSF dispersion for an optically thin atmosphere, the SAA can be used even in this

AMTD
3, 1645–1705, 2010

case. Moreover, for an optically thin atmosphere we can consider the dispersions of the PSF for molecular and aerosol scattering independently.

The dispersion of the scattered component of the PSF when light propagates from the source at the height Hover land is estimated with the SAA as (Zege et al., 1991)

$$V^s = \frac{\int_0^H \sigma(h)\theta_2(h)h^2 dh}{2\left[1-\exp\left(-\int_0^H \sigma(h)dh\right)\right]}, \quad \text{(A1)}$$

where $\sigma(h)$ and $\theta_2(h)$ are profiles of the altitude distribution of the scattering coefficient and of the second angular moment of the phase function, respectively.

For our rough estimations the altitude profile of the molecular scattering coefficient in the atmosphere can be taken as the exponential (Elterman, 1986)

$$\sigma_{\text{mol}}(h) = \sigma_{\text{mol}}(0)\exp(-\alpha_{\text{mol}}h), \quad \text{(A2)}$$

with $\alpha_{\text{mol}} = 1/8\text{km}^{-1}$ (Santer et al., 2000). The total optical thickness of the molecular atmosphere is

$$\tau_{\text{mol}} = \int_0^\infty \sigma_{\text{mol}}(h)dh = \sigma_{\text{mol}}(0)/\alpha_{\text{mol}}. \quad \text{(A3)}$$

Let us take, for instance, the altitude profile of the aerosol extinction coefficient ε_{aer} in the lower troposphere layer ($h < 2$ km) that contains the major part of aerosol in the form

$$\varepsilon_{\text{aer}} = \varepsilon_{\text{aer}}(0)\exp(-\alpha_{\text{aer}}h), \quad \text{(A4)}$$

where $\varepsilon_{\text{aer}}(0) = 3.91/\text{S}_\text{m}$, S_m is the meteorological visibility range at the atmosphere ground-level, $\alpha_{\text{aer}} = 0.92\,\text{km}^{-1}$ (WMO, 1986).

The total optical thickness of the aerosol atmosphere is

$$\tau_{\text{aer}} = \int_0^\infty \varepsilon_{\text{aer}}(h)\,dh = \varepsilon_{\text{aer}}(0)/\alpha_{\text{aer}}. \tag{A5}$$

From Eqs.(A1)–(A3) it follows that the dispersion of the PSF due to the scattering in the molecular atmosphere is

$$V_{\text{mol}}(H) = \frac{\tau_{\text{mol}}\theta_{2,\text{mol}}}{\alpha_{\text{mol}}^2}\Psi_{\text{mol}}(H), \tag{A6}$$

where

$$\Psi_{\text{mol}}(H) = \frac{\left[1 - \left(1 + \alpha_{\text{mol}}H + \frac{(\alpha_{\text{mol}}H)^2}{2}\right)\exp(-\alpha_{\text{mol}}H)\right]}{1 - \exp\left[-\tau_{\text{mol}}(1 - \exp(-\alpha_{\text{mol}}H))\right]}. \tag{A7}$$

With regard to Eqs. (A1), (A4), (A5) for the PSF dispersion due to the scattering in the aerosol atmosphere we get:

$$V_{\text{aer}}(H) = \frac{\omega_{\text{aer}}\tau_{\text{aer}}\theta_{2,\text{aer}}}{\alpha_{\text{aer}}^2}\Psi_{\text{aer}}(H), \tag{A8}$$

where ω_{aer} is the single scattering albedo for aerosol.

For the molecular atmosphere it can be taken $\theta_{2,\text{mol}} \approx 1$ while for the aerosol atmosphere with *Continental* aerosol $\theta_{2,\text{aer}} \approx 0.7$.

Let us consider atmosphere with $\tau_{\text{aer}} < 1$ and $\tau_{\text{mol}} < 1$. Then we have from Eqs. (A6) and (A8):

$$V_{\text{mol}}(H) \approx \frac{\theta_{2,\text{mol}}}{\alpha_{\text{mol}}^2}\Psi^*_{\text{mol}}(H), \tag{A9}$$

where

$$\Psi^*_{\mathrm{mol}}(H) = \frac{\left[1 - \left(1 + \alpha_{\mathrm{mol}}H + \frac{(\alpha_{\mathrm{mol}}H)^2}{2}\right)\exp(-\alpha_{\mathrm{mol}}H)\right]}{1 - \exp(-\alpha_{\mathrm{mol}}H)}, \tag{A10}$$

and

$$V_{\mathrm{aer}}(H) \approx \frac{\theta_{2,\mathrm{aer}\,r}}{\alpha^2_{\mathrm{aer}}}\Psi^*_{\mathrm{aer}}(H), \tag{A11}$$

i.e. the PSF dispersion is practically independent of the atmospheric optical thickness. It means that the area with adjacent pixels that affects the signal from the pixel under observation is practically the same for clouds and underlying land surface.

In the case of the satellite sensor, when $\alpha_{\mathrm{mol}}H \gg 1, \alpha_{\mathrm{aer}}H \gg 1$, from (A9) and (A11) we get:

$$V_{\mathrm{mol}} = \frac{\theta_{2,\mathrm{mol}}}{\alpha^2_{\mathrm{mol}}}, \qquad V_{\mathrm{aer}} = \frac{\theta_{2,\mathrm{aer}}}{\alpha^2_{\mathrm{aer}}}. \tag{A12}$$

Figure A1 shows dispersions $V_{\mathrm{mol}}(H)$ and $V_{\mathrm{aer}}(H)$ as functions on a sensor altitude H. As seen, in the case of observations from a helicopter (H=500 m) the effective area of a underling surface that contributes in the registered signal because of the scattering in the aerosol atmosphere is about 0.03 km^2, while such area is about 0.3–0.5 km^2 at observation from aircraft at the flight altitude (H=2–3 km) and achieves 1 km^2 for observation from satellite or aircraft at high altitudes. The molecular scattering in atmosphere leads to the increasing the effective surface area that contributes into the registered signal from considered pixel and this influence is expected to be more pronounced in the shortwave part of spectrum with the increasing the contribution of the molecular scattering.

Thus, the presence of a cloud (snow, sand with high albedo) in some pixel affects signals registered from the nearby pixels up the distance about 1 km because of the

scattering in aerosol atmosphere and at a few kilometers because of molecular scattering. Note, that fulfilled estimations are in a good agreement with results reported in (Dave, 1980; Kaufman, 1985) and with requirements to the size of an area for the calibration of satellite optical sensors. Let us emphasize that the PSF dispersion is determined only by the scattering in atmosphere and, as a direct consequence, practically does not depend on the satellite altitude.

Acknowledgements. This work benefited through numerous discussions and collaboration with many scientists. In particular, we are grateful to W. von Hoyningen-Huene, J. P. Burrows, and A. P. Ivanov.

This work was partially done in the framework of the Russia-Belarus program "Cosmos-NT". Authors are thankful to ESA for providing MERIS data used in this research.

References

Chaikovskaya, L. I., Katsev, I. L., Prikhach, A. S., and Zege, E. P.: Fast code to compute polarized radiation transfer in the atmosphere-ocean and atmosphere-earth systems, IGARSS'99, IEEE, International Geoscience and Remote Sensing Symposium, Congress Centrum Hamburg Remote Sensing of the System Earth a Challenge for the 21th Century Proceedings-CD-ROM, Hamburg, Germany, 1999.

Dave, J. V.: Effect of atmospheric conditions on remote sensing of a surface nonhomogeneity, Photogramm. Eng. Rem. S., 46, 1173–1180, 1980.

Elterman, L.: UV, Visible and IR Attenuation to 50km, Report AIGRL-68-0153, Bedford, Mas, 1986.

Katsev, I. L., Prikhach, A. S., Zege, E. P, Ivanov, A. P., and Kokhanovsky, A. A.: Iterative procedure for retrieval of spectral aerosol optical thickness and surface reflecatnce from satellite data using fast radiative transfer code and its application to MERIS measurements, in Satellite aerosol remote sensing over land, edited by: Kokhanovsky, A. A. and de Leeuw, G., Springer-Praxis, Berlin, Germany, 101–134, 2009.

Kaufman, Y. J.: The atmospheric effect on the separability of field classes measured from satellites, Remote Sens. Environ., 18, 21–34, 1985.

Kaufman, Y. J., Tanre, D., Gordon, H. R., Nakajima, T., Lenoble, J., Frouin, R., Grassl, H., Herman, B. M., King, M. D., and Teillet, P. M.: Passive remote sensing of tropospheric aerosol and atmospheric correction for the aerosol effect, J. Geophys. Res., 102, 16 815–16 830, 1997.

Kokhanovsky, A. A., Breon, F.-M., Cacciari, A., Carboni, E., Diner, D., Di Nicolantonio, W., Grainger, R. G. Grey, W. M. F., Holler, R., Lee, K.-H., Li, Z., North, P. R. J., Sayer, A., Thomas, G., von Hoyningen-Huene, W.: Aerosol remote sensing over land: A comparison of satellite retrievals using different algorithms and instruments, Atmos. Res., 85, 372–294, 2007.

Kokhanovsky, A. A., Deuzé, J. L., Diner, D. J., Dubovik, O., Ducos, F., Emde, C., Garay, M. J., Grainger, R. G., Heckel, A., Herman, M., Katsev, I. L., Keller, J., Levy, R., North, P. R. J., Prikhach, A. S., Rozanov, V. V., Sayer, A. M., Ota, Y., Tanré, D., Thomas, G. E., and Zege, E. P.: The inter-comparison of major satellite aerosol retrieval algorithms using simulated intensity and polarization characteristics of reflected light, Atmos. Meas. Tech. Discuss., 2, 3369–3439, 2009, http://www.atmos-meas-tech-discuss.net/2/3369/2009/.

Kokhanovsky, A. A., Cornet, C., Duan, M., Emde, C., Katsev, I. L., Labonnote, L.-C., Min, Q., Nakajima, T., Ota, Y., Prikhach, A. S., Rozanov, V. V., Yokota, T., and Zege, E. P.: Benchmark results in vector radiative transfer, JQSRT, doi:10.1016/j.jqsrt.2010.03.005, 2010.

Lenoble, J.: Radiative Transfer in Scattering and Absorbing Atmospheres: Standard Computational Procedures, A. Deepak Publishing, Hampton, Virginia, USA, 314 pp., 1985.

Richter, R.: On the in-flight absolute calibration of high spatial resolution spaceborne sensors using small ground targets, Int. J. Remote Sens., 18, 2827–2833, 1997.

Santer, R., Ramon, D., Vidot, J., Dilligeard, E., et al.: Atmospheric product over land for MERIS level 2. MERIS Algorithm Theoretical Basis Document, ATBD 2.15, 2000.

Sobolev, V. V.: Scattering of Light in Planetary Atmosphere, Pergamon, New York, USA, 1975.

Tynes, H., Kattawar, G. W., Zege, E. P., Katsev, I. L., Prikhach, A. S., and Chaikovskaya, L. I.: Monte Carlo and multicomponent approximation methods for vector radiative transfer by use of effective Mueller matrix calculations, Appl. Opt., 40, 400–412, 2001.

von Hoyningen-Huene, W., Freitag, M., and Burrows, J. B.: Retrieval of aerosol optical thickness over land surfaces from top-of-atmosphere radiance, J. Geophys. Res., 108(D9), 4260, doi:10.1029/2001JD002018, 2003.

WMO International Association for Meteorology and Atmospheric Physics Radiation Commis-

sion: A preliminary cloudless standard atmosphere for radiation computation, World Climate Program, WCP-112 WMOyTD-#24 ~World Meteorological Organisation, Geneva, 1986.
Zege, E. P., Ivanov, A. P., Katsev, I. L.: Image Transfer through a Scattering Medium, Springer-Verlag, 349 pp., Heidelberg, Germany, 1991.

Table 1. Coefficients of the linear regression between AERONET data and the retrieved AOT values for different situations.

Cloudless, %	Belsk (Poland)	Zvenigorod (Russia)
< 10%	y=0.8761 x+ 0.0805	y= 0.848 x+0.0398
10%–50%	y=0.7898 x+0.1898	y=0.6962 x+0.2
> 50%	y=0.1915 x+0.413	y=0.4364 x+0.5356

Table 2. Coefficients of the linear regression between the AERONET data and the retrieved AOT values with additional discrimination of pixels adjacent to the cloudy pixel.

Cloudless, %	Belsk (Poland)	Zvenigorod (Russia)
< 10%	y=0.8606 x + 0.0793	y = 0.8257 x + 0.0335
10%–50%	y=0.7951 x+0.1476	y=0.8581 x+0.0744
> 50%	y=0.4238 x + 0.2628	y=1.2798 x + 0.1382

AMTD
3, 1645–1705, 2010

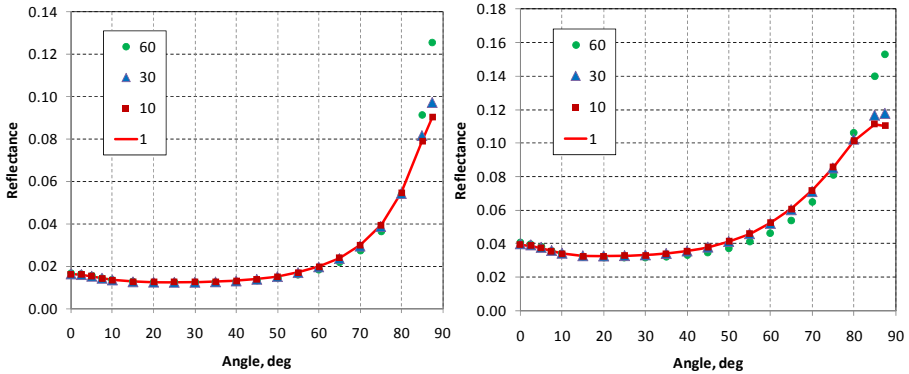

Fig. 1. The reflectance for the aerosol layer computed with RAY at different truncation angles given in the legend. Aerosol model *Continental*, the normal incidence; r=0.2 (left) and 0.5 (right).

AMTD
3, 1645–1705, 2010

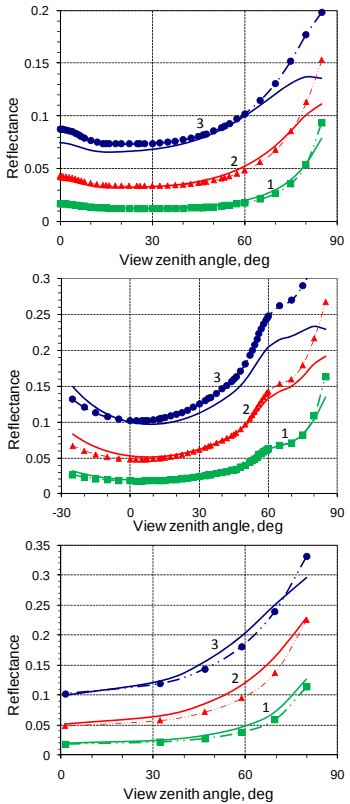

Fig. 2. Reflectance R_1 (μ, μ_0, φ) versus the view zenith angle at different zenith and azimuth Sun positions: sun angle is 0˚ (top); Sun angle 60˚, azimuth 180˚ (middle); Sun angle 60˚, azimuth 90˚ (bottom). Aerosol model *Continental*, the layer optical thickness is equal to 0.2 (1), 0.5 (2), 1 (3). Computations with RAY (solid lines) and MSA (dashed lines with signs) are shown.

AMTD
3, 1645–1705, 2010

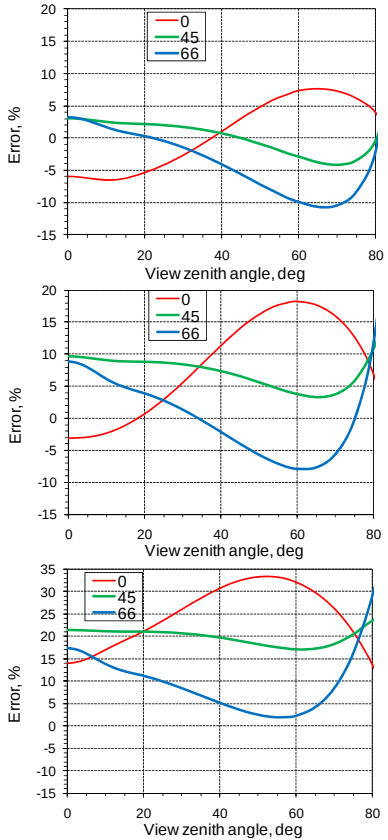

Fig. 3. Errors of the MSA computations of the reflectance from layers with *Continental* aerosol at normal incidence dependent on the view zenith angle at the layer optical thickness equal to 0.2 (top), 0.5 (middle), 1.0 (bottom). Data for different cut angles are given in red (0°), green (45°) and blue (66°).

AMTD
3, 1645–1705, 2010

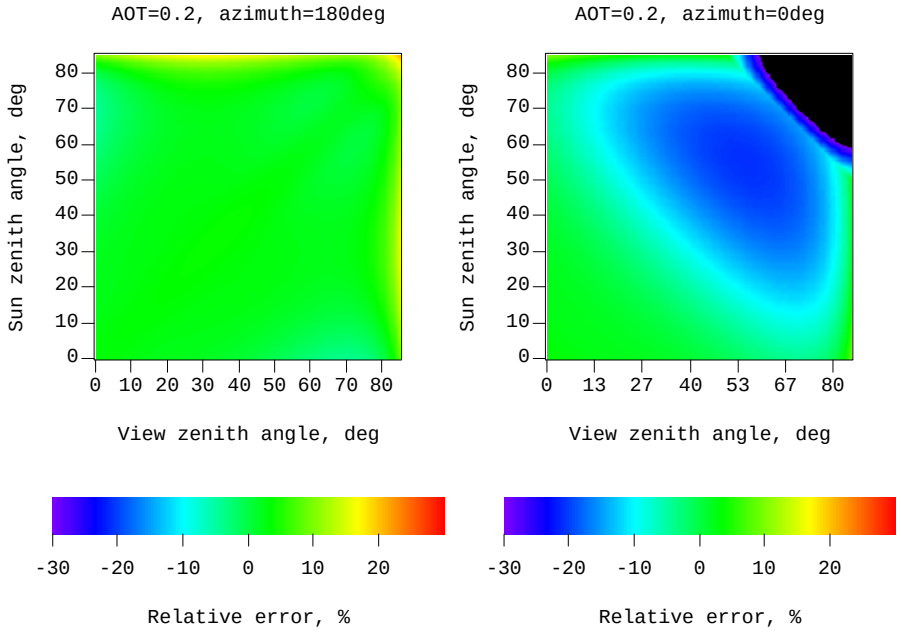

Fig. 4. Relative errors of the reflectance from the layer "1" at the layer optical thickness equal to 0.2.

AMTD
3, 1645–1705, 2010

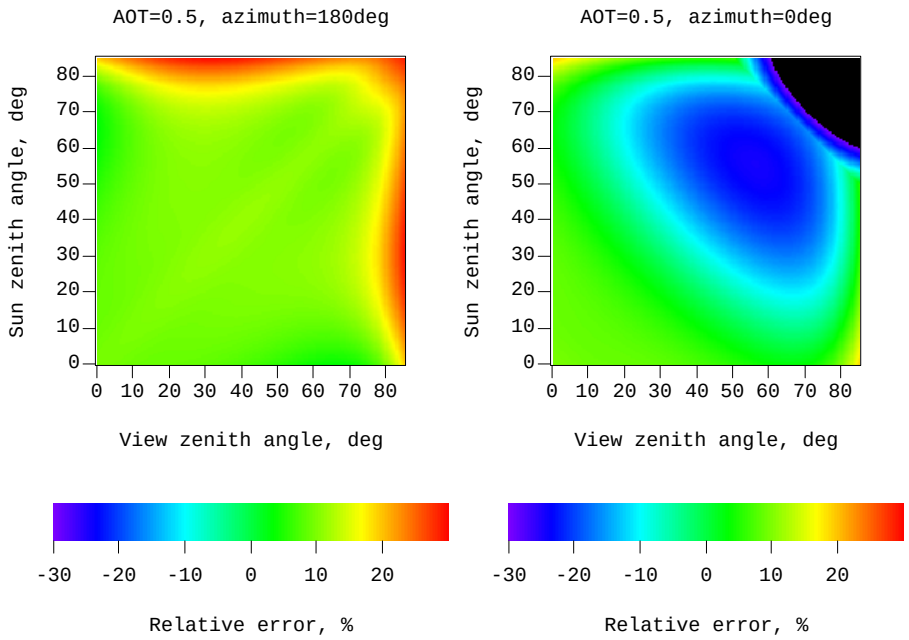

Fig. 5. Relative errors of the reflectance from the layer "1" at the layer optical thickness equal to 0.5.

AMTD
3, 1645–1705, 2010

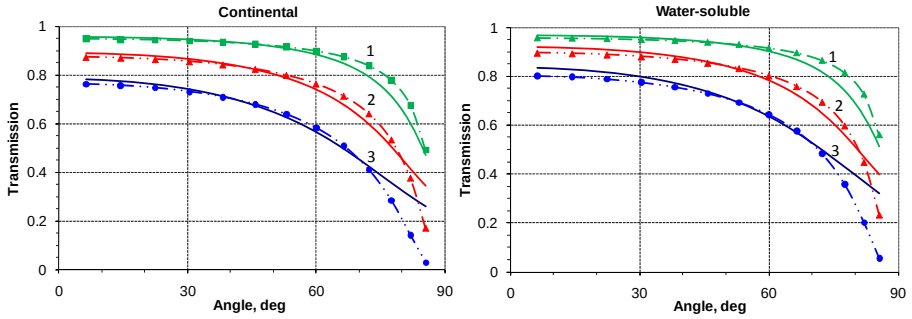

Fig. 6. The transmission coefficient $t_1(\mu_0)$ versus the Sun zenith angle ϑ_0= across μ_0 at τ_1=0.2 (1), 0.5 (2) and 1 (3) for the *Continental* and *Water-soluble* aerosols. Computations with RAY (solid lines) and with Eq. (34) (signs) are shown.

AMTD
3, 1645–1705, 2010

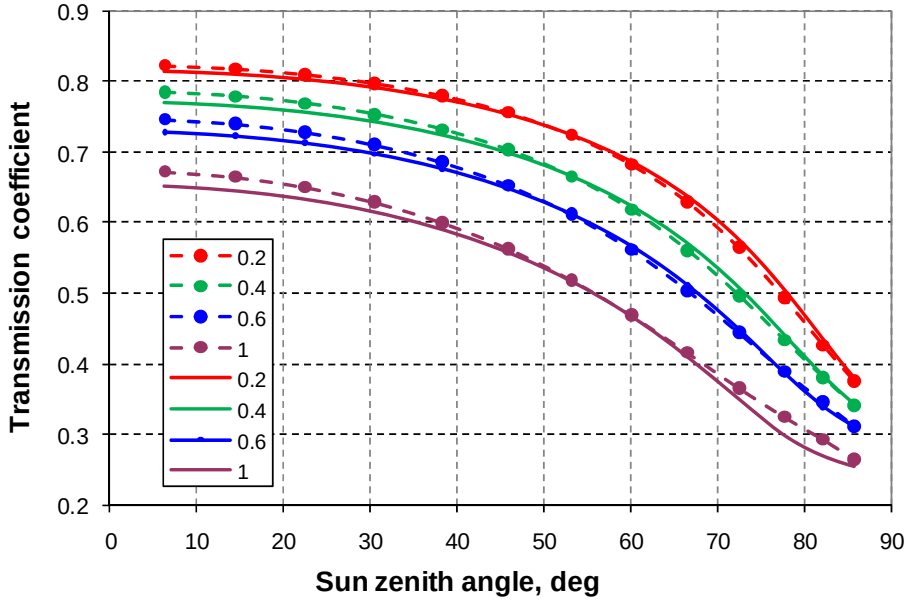

Fig. 7. The atmosphere transmission coefficient (32) versus Sun zenith angle. The atmosphere upper layer "2" has the molecular optical thickness τ_{mol} and contains aerosol H_2SO_4 with τ=0.0255; the lower layer "1" contains the *Continental* aerosol with optical thickness τ that is given in the legend. Computations with Eqs. (32)–(34) (dashed lines), the accurate computations with the RAY code (solid lines) are shown.

AMTD
3, 1645–1705, 2010

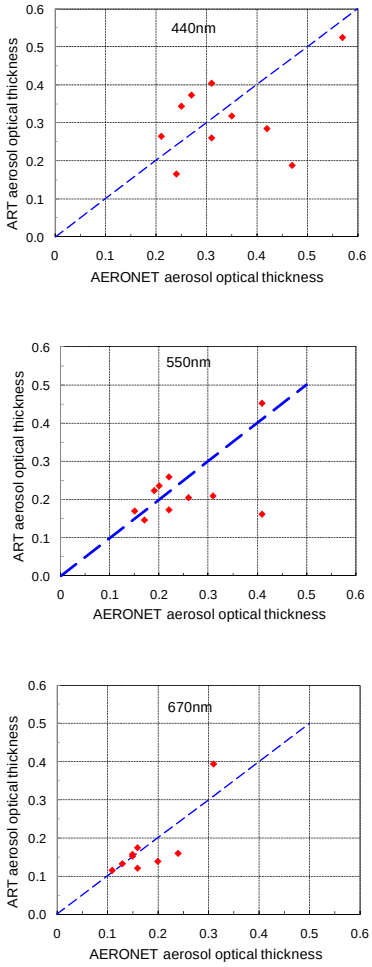

Fig. 8. The AOT retrieved with the ART code versus AERONET AOT at λ=440 nm, 550 nm, and 670 nm.

AMTD
3, 1645–1705, 2010

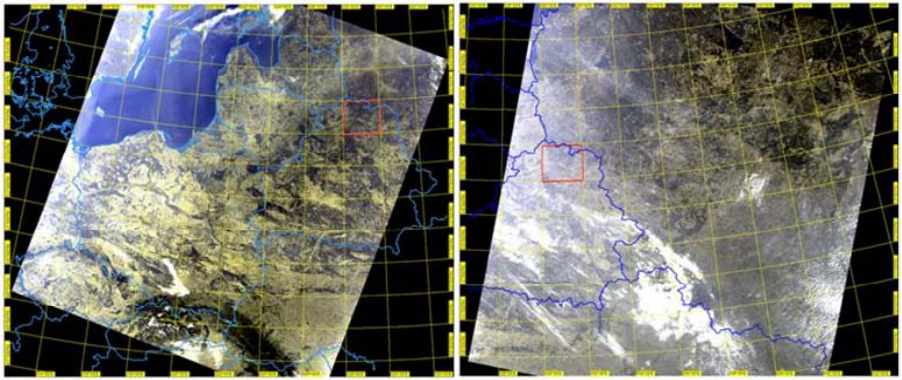

Fig. 9. Composite RGB images: MERIS on ENVISAT platform; 11 October 2005 (left) and 1 May 2006 (right).

AMTD

3, 1645–1705, 2010

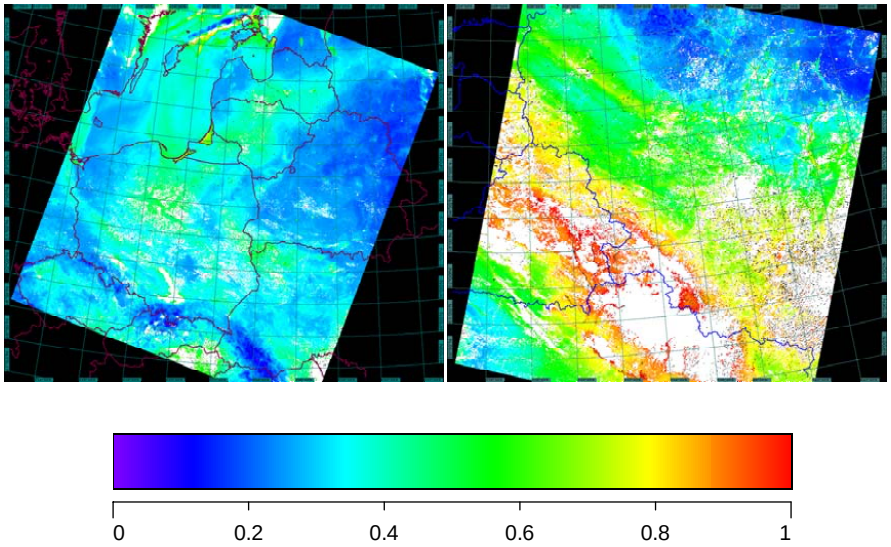

Fig. 10. AOT distribution over presented in Fig. 9 regions retrieved with the FAR code.

AMTD
3, 1645–1705, 2010

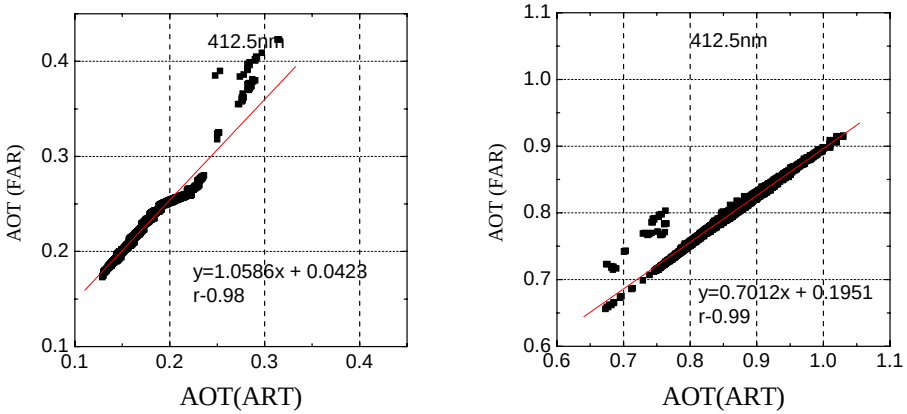

Fig. 11. Correlation between values of AOT at 412.5 nm retrieved with the FAR and ART codes.

AMTD
3, 1645–1705, 2010

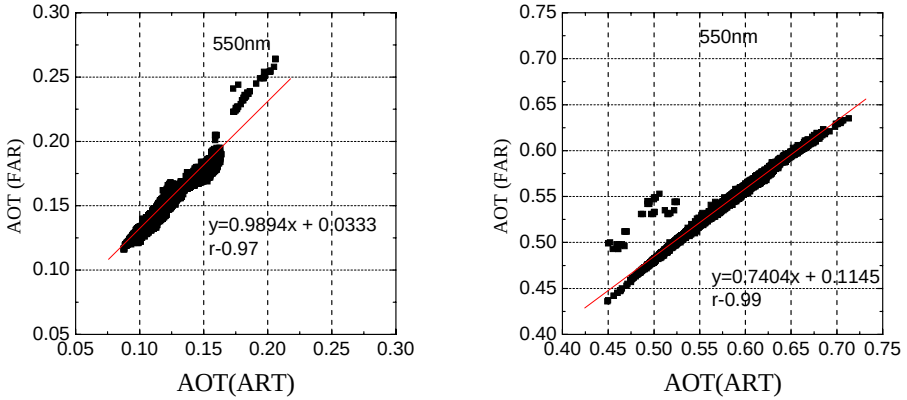

Fig. 12. The same as in Fig. 11 except for the wavelength of 550 nm.

AMTD
3, 1645–1705, 2010

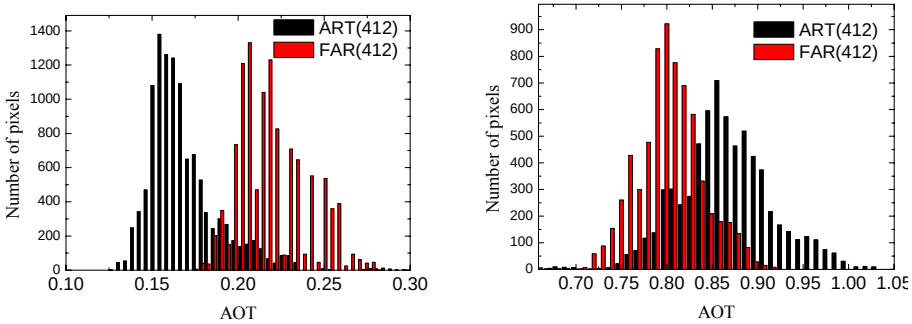

Fig. 13. Histograms of the distributions of the AOT at the wavelength 412.5 nm retrieved with the FAR and ART codes from MERIS on ENVISAT data for the areas marked in Fig. 9.

AMTD
3, 1645–1705, 2010

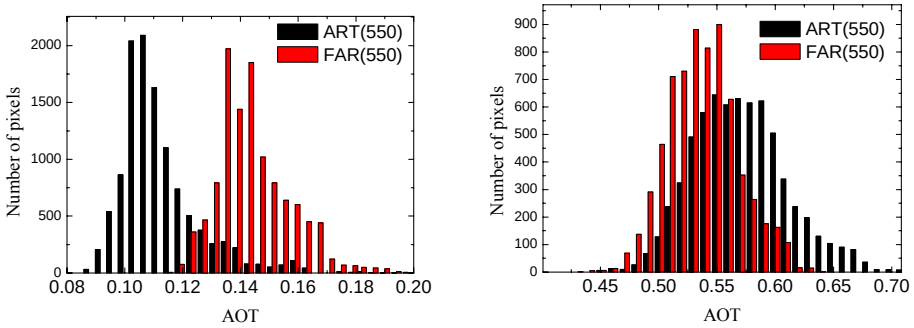

Fig. 14. Histograms of the distributions of the AOT at the wavelength 550 nm retrieved with the FAR and ART codes from MERIS on ENVISAT data for the areas marked in Fig. 9.

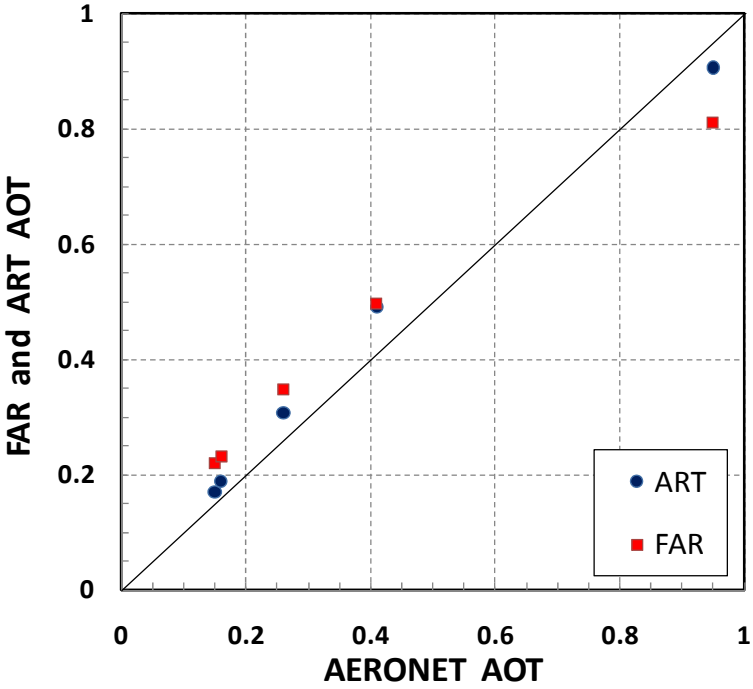

Fig. 15. Correlation between values of AOT at 412.5 nm retrieved with the FAR and ART codes.

AMTD
3, 1645–1705, 2010

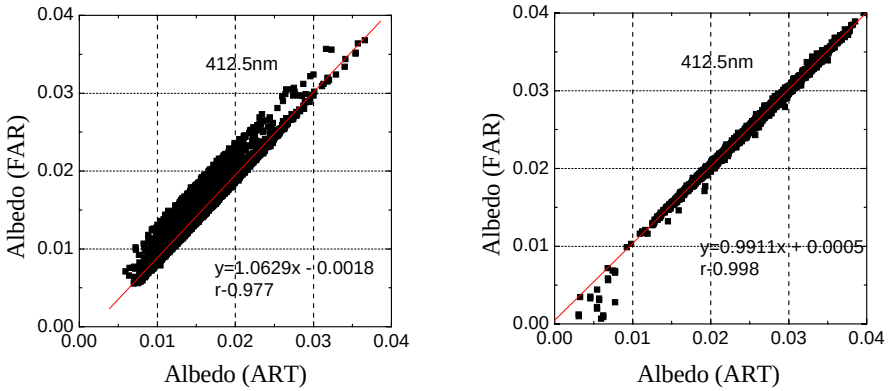

Fig. 16. Correlation between the ART and FAR retrieved albedo of land at 412.5 nm for clear (left) and turbid (right) atmospheres (see Fig. 9).

AMTD
3, 1645–1705, 2010

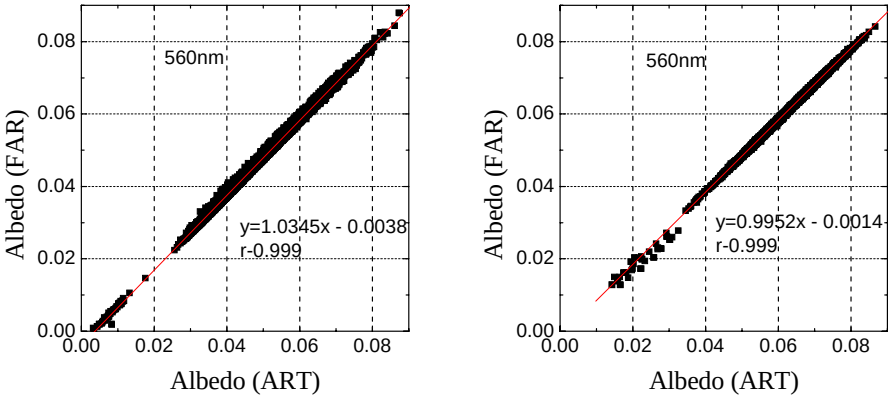

Fig. 17. Correlation between the ART and FAR retrieved albedo of land at 560 nm for clear (left) and turbid (right) atmospheres (see Fig. 9).

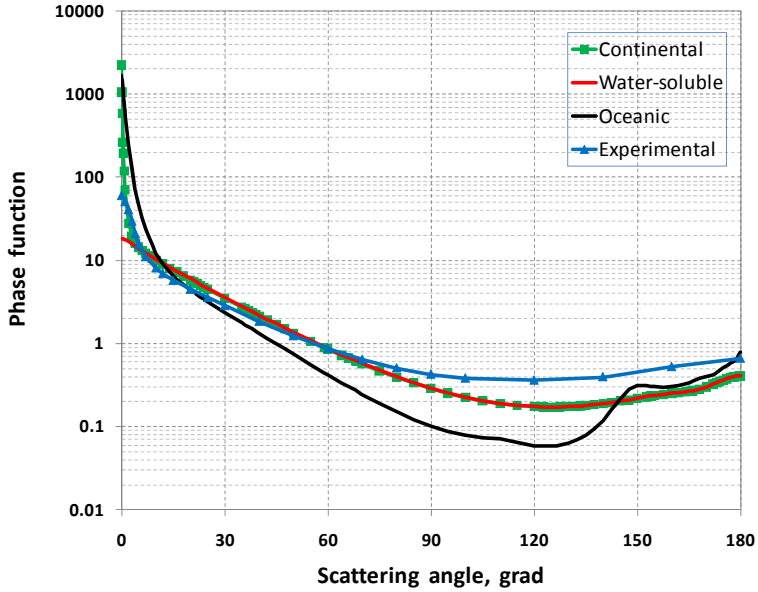

Fig. 18. Phase functions of different aerosol types at λ=550 nm.

AMTD
3, 1645–1705, 2010

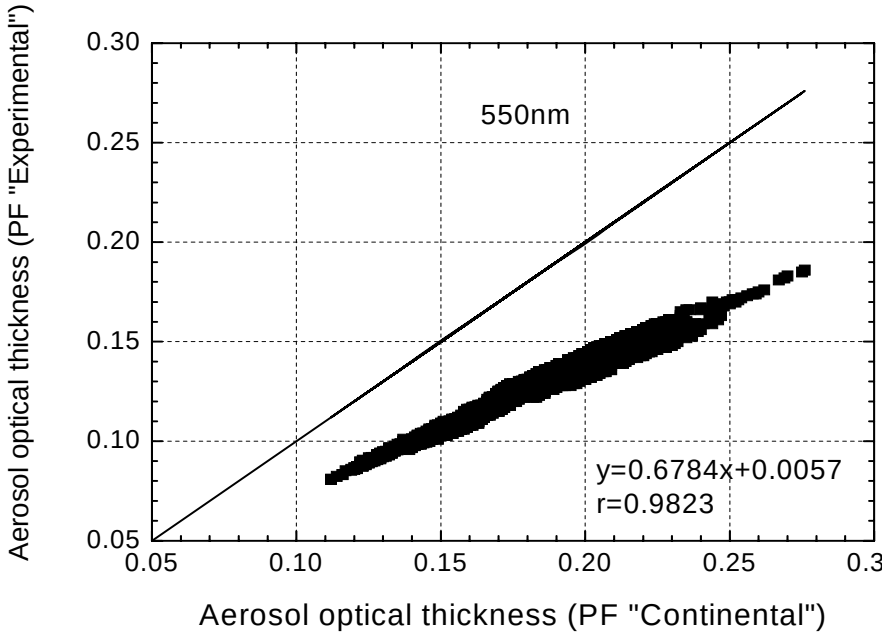

Fig. 19. Comparison of the AOTs (550 nm) retrieved by the ART algorithm using *Continental* and *experimental* phase functions. *r* is the correlation coefficient.

AMTD
3, 1645–1705, 2010

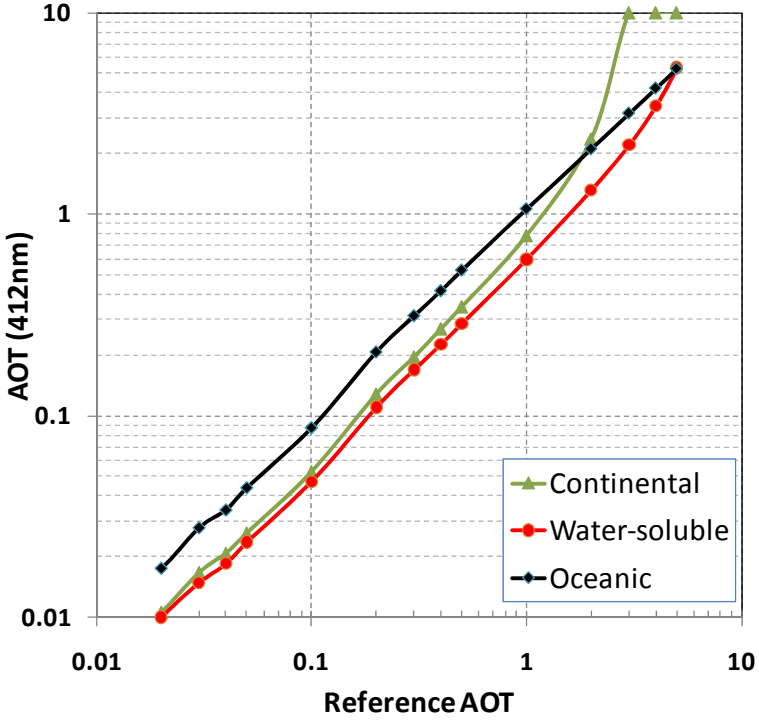

Fig. 20. Values of the AOT at λ=550 nm retrieved by the ART for different aerosol types from the simulated spectral reflectance at the TOA.

AMTD
3, 1645–1705, 2010

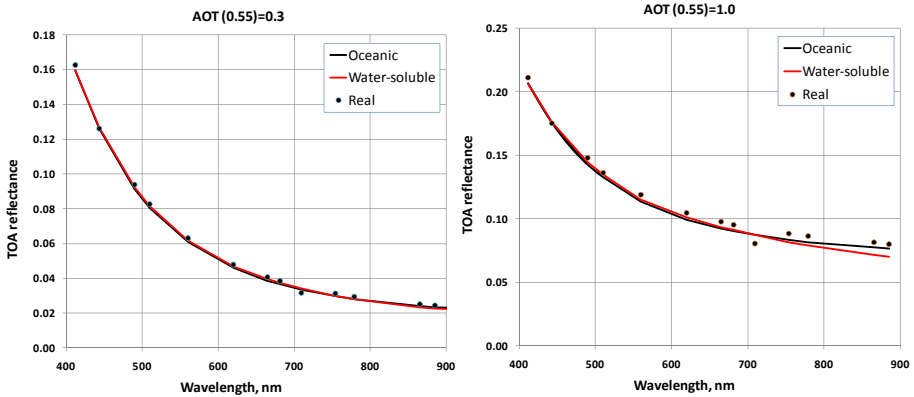

Fig. 21. Reflectance at the TOA computed using code RAY with the retrieved AOT values and atmosphere models used for the retrieval for the AOT equal to 0.3 (left) and 1.0 (right) at λ=550 nm.

AMTD
3, 1645–1705, 2010

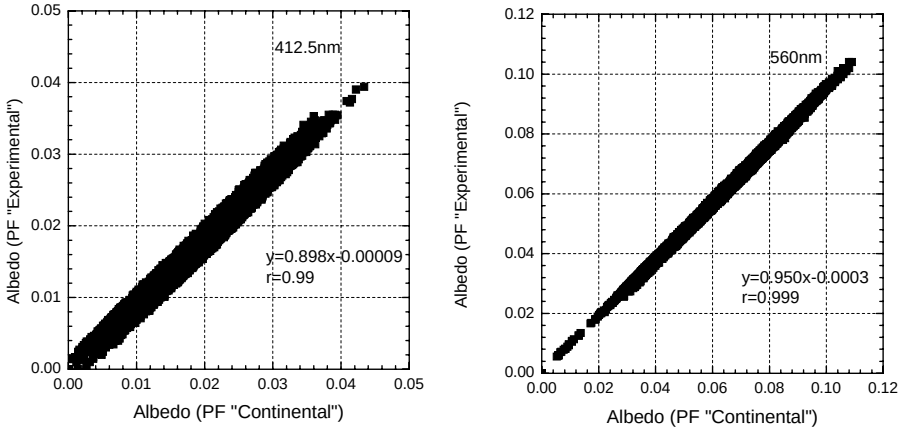

Fig. 22. Surface albedo retrieved with the experimental phase function versus the same value retrieved with the *Continental* phase function at wavelengths of 412.5 nm (left) and 560 nm (right). *r* is the correlation coefficient.

AMTD
3, 1645–1705, 2010

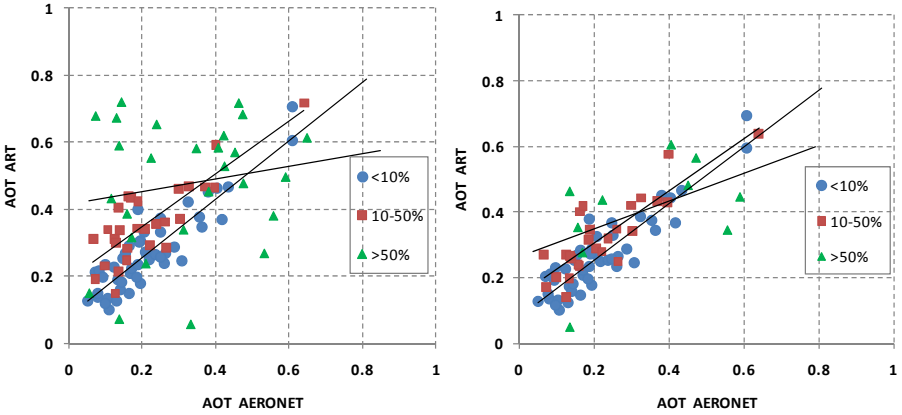

Fig. 23. The satellite-derived AOT values at λ=440 nm for region of Belsk (Poland) versus AERONET AOT. Different signs are given for cloud situations with numbers of pixels identified as cloudy less than 10%, in range 10–50%, and more than 50% (see the legends). The lines show the linear regressions between the retrieved AOT values and AERONET data. MERIS data are averaged over a circle with the radius of 20 km with the center in the pixel where AERONET measurements were performed (left picture). The same but with additional discarding of pixels in the square 5×5 with cloudy pixel in the center (right picture).

AMTD
3, 1645–1705, 2010

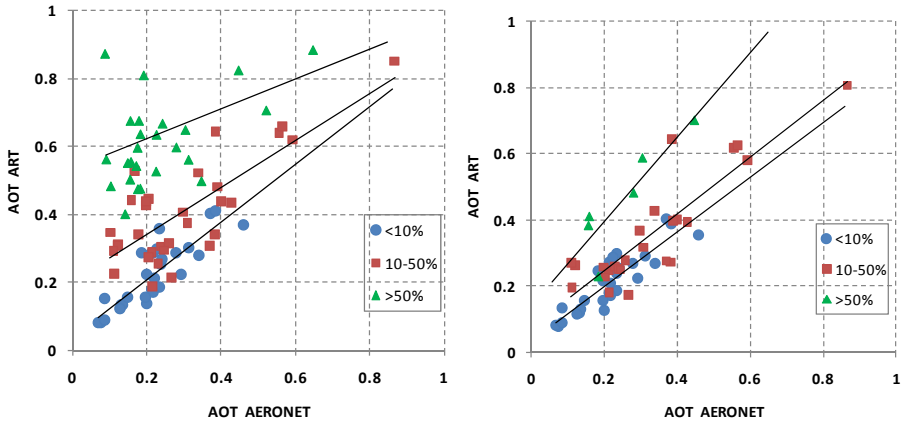

Fig. 24. The same as in Fig. 23 except for the region of Zvenigorod (Russia).

AMTD
3, 1645–1705, 2010

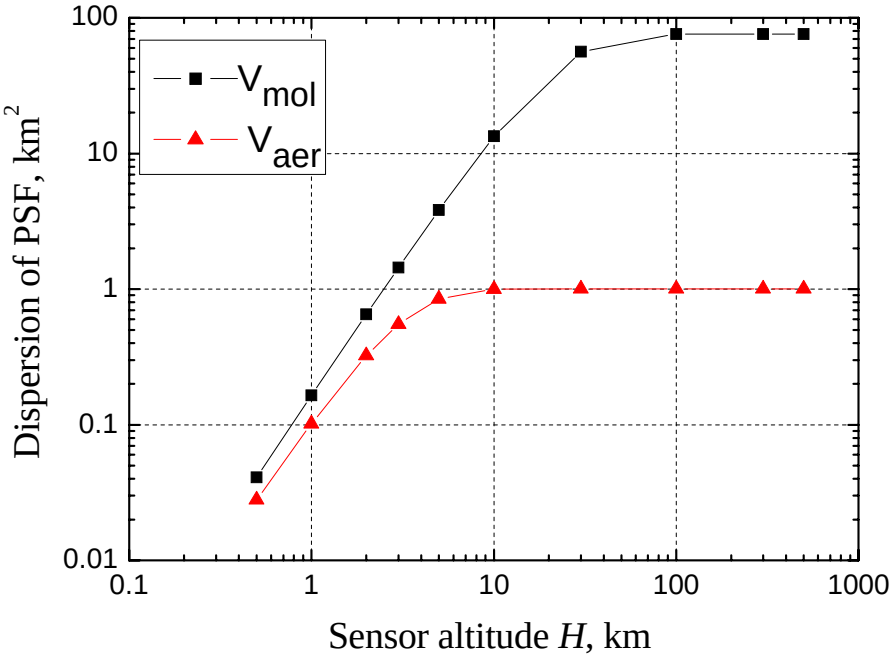

Fig. A1. Dependence of the dispersions V_{mol} (H) and V_{aer} on the sensor altitude.

AMTD
3, 1645–1705, 2010